PHYSICOCHEMICAL CHARACTERIZATION OF ASPHALTENES

A Thesis

by

ANDREAS ADI PRAKOSO

Submitted to the Office of Graduate and Professional Studies of
Texas A&M University
in partial fulfillment of the requirements for the degree of

MASTER OF SCIENCE

Chair of Committee,	Berna Hascakir
Committee Members,	Hadi Nasrabadi
	Yuefeng Sun
Head of Department,	A. Daniel Hill

May 2016

Major Subject: Petroleum Engineering

ABSTRACT

This work proposes the study on physicochemical characterization of crude oils and their asphaltenes to understand the destabilization mechanism of asphaltenes. Knowledge on the molecular-scale interactions between components of crude oil is vital for the assessment of potential reserves and mitigation efforts of asphaltene-related problems. 11 heavy oil and bitumen samples from various regions of the world were subjected to characterization to attain universal yet simple correlations that are applicable under operating conditions. Comprehensive physicochemical analysis of the samples were performed through density and viscosity measurements of the crude oil, Saturates, Aromatics, Resins, and Asphaltenes (SARA) fractionation, Fourier Transform InfraRed (FTIR) spectroscopy analysis, elemental analysis, solubility profile assessment, and onset asphaltene precipitation (OAP) tests on the crude oil samples. Furthermore, two different types of asphaltenes were examined; n-pentane and n-heptane insolubles. Accordingly, density, zeta potential, and cluster size measurements, as well as high resolution microscopy imaging techniques, were conducted on these asphaltene samples to support the asphaltene stability and onset precipitation test results. The results have revealed that heteroatoms contained within the crude oils and asphaltenes play an important role in defining the physicochemical characteristics of crude oil. In particular, oxygen and metal (mostly V and Ni) functional groups were found to contribute significantly towards asphaltene stability and polarity. Additionally, this study has established that the presence of impurities in the saturates fraction causes it to have a destabilizing power towards

asphaltenes. Thus, higher concentration of saturate fraction in the crude oil may pose higher risks of asphaltene-related issues. Moreover, it is highly recommendable that OAP experiments are conducted by using the crude oil's own saturate fraction to achieve better accuracy and provide representative results of actual reservoir conditions.

DEDICATION

I dedicate this thesis to my parents, brothers, and friends who have given me their full support throughout my life.

ACKNOWLEDGEMENTS

I would like to thank Dr. Berna Hascakir for her continuous guidance and support throughout my research. Without her encouragements, I would not have been able to realize my full potential and reach such great heights with this study. I am also grateful to Dr. Hadi Nasrabadi and Dr. Yuefeng Sun for their willingness to serve as my committee members.

A special thanks to Abhishek Punase who have helped me in countless occasions during my research. I would also like to specifically thank Kristina Klock for assisting me with some of the laboratory measurements. Moreover, I would like to express my deepest gratitude to all the members of the Heavy Oil, Oil shales, Oil sands, and Carbonate Analysis and Recovery Methods (HOCAM) research group for their help and support.

I would like to extend my gratitude to Chevron, especially to Dr. Cesar Ovalles and Estrella Rogel, for their assistance in conducting the elemental analysis and solubility profile experiments. Furthermore, I am grateful to all the staff and faculty members of Texas A&M University who have shared their insights and also aided me in conducting lab measurements. Financial support from the Society of Petroleum Engineers (SPE) is also greatly appreciated.

Lastly, I am thankful to all the support and motivation that my family and friends have given me throughout my life.

NOMENCLATURE

AFM	Atomic Force Microscopy
ASTM	American Society for Testing and Materials
ATR	Attenuated Total Reflectance
DSC	Differential Scanning Calorimetry
EDS	Energy Dispersive X-ray Spectroscopy
ELSD	Evaporative Light Scattering Detector
ESI-MS	ElectroSpray Ionization – Mass Spectrometry
FTIR	Fourier Transform InfraRed
HPLC	High Performance Liquid Chromatography
nC_5	n-pentane
nC_7	n-heptane
NMR	Nuclear Magnetic Resonance
SARA	Saturates, Aromatics, Resins, Asphaltenes
SEM	Scanning Electron Microscopy
TDS	Total Dissolved Solids
TGA	ThermoGravimetric Analysis
wt%	weight percent

TABLE OF CONTENTS

Page

LIST OF FIGURES

Page

LIST OF TABLES

Page

CHAPTER I

INTRODUCTION

Asphaltenes are defined as the fraction of crude oil that are insoluble in normal alkanes (aliphatic hydrocarbons) but soluble in aromatic solvents (Speight 2006). Asphaltenes are also known to contain the heaviest and the most polar components of crude oil (Li and Firoozabadi 2010). Because of these polar elements, asphaltene molecules have an inherent ability to self-associate between themselves to create larger and heavier clusters (Speight 2014). When the aggregates become too heavy, asphaltene molecules then precipitate out of the crude oil and transition into a solid phase. Because it is a phase related issue, pressure, temperature, and compositional changes are known as the main cause of asphaltene precipitation during production (Mullins et al. 2007; Speight and Long 1996).

Asphaltene precipitation can essentially occur at all stages of petroleum production, which can lead to various undesired problems (Leontaritis 1989; Kokal and Sayegh 1995; Izquierdo and Rivas 1997). Inside the reservoir, asphaltene buildup can significantly reduce permeability and productivity through pore blockage, alter wettability from water-wet to oil-wet, and increase oil viscosity (Khalifeh et al. 2013; Leontaritis et al. 1994; Seifried et al. 2013; Uetani 2014). The accumulation of asphaltene can also damage well tubular, downhole equipment, and pumps (Alkafeef et al. 2005; Limanowka et al. 1999). Furthermore, previous cases of flow restriction in pipelines and production

facilities have been reported to be caused by asphaltene deposition (Wylde and Slayer 2010; Thawer et al. 1990).

Chemical composition of asphaltenes vary greatly depending on the precipitation conditions (Ortega et al. 2015; McLean and Kilpatrick 1997; Dabir et al. 1996). Previous studies have found that asphaltene deposits obtained from the wellbore have different characteristics compared to synthetically precipitated asphaltenes through solvent addition (Klein et al. 2006; Rogel, Miao, et al. 2015). However, the impracticalities associated with generating such high pressure and temperature makes precipitation by solvents much more feasible for extensive characterization of asphaltenes (Gawel and Speight 2010). Hence, simulation of asphaltene precipitation behavior is conducted through onset asphaltene precipitation experiments by deliberately altering the chemical composition of the crude oil with addition of n-alkanes (Akbarzadeh et al. 2004).

Onset precipitation is based on solubility of asphaltenes in different solvents (Speight 1994; Speight et al. 1984). The amount of precipitated asphaltenes decreases as the carbon number of the precipitating alkane increases (Kokal et al. 1992; Buenrostro-Gonzalez et al. 2004). For instance, the weight of the n-heptane insoluble fractions of crude oil should be less than the n-pentane insoluble fractions (Speight 2006). Branching of the alkane solvent also results in more asphaltene yield (Brons and Yu 1995). This precipitating behavior is found to be related to the solvent power of hydrocarbon solvents, or otherwise known as the solubility parameter (Mitchell and Speight 1973; Hildebrand 1919). As the solubility parameter of non-polar solvents increases, the solvent is able to dissolve larger proportions of the crude oil while leaving behind lesser amounts of the

heavier and more complex fractions of asphaltenes. In accordance with this theory, Ortega et al. (2015) have found that asphaltenes precipitated by n-heptane (nC_7) are more polar, more viscous, and have higher molecular weight and density compared to n-pentane (nC_5) asphaltenes. As a side note, they also mentioned that n-heptane asphaltene separation techniques, e.g. ASTM D3279, D4124, and D6560, are mainly chosen due to their high reproducibility while n-pentane separation, e.g. ASTM D893 and D2007, are more similar to industrial deasphalting operations that uses C4-C6 condensates (ASTM 2012a, 2009, 2012b, 2014, 2011). Hence, the identification of asphaltenes (n-alkane insolubles) used in every characterization studies based on their precipitating solvent become crucial to understand the applicability of the research results.

The popular belief is that asphaltene molecules are stable colloids suspended in crude oils or bitumen (Ravey et al. 1988; Ramos et al. 2001; Mullins et al. 2013; Goual et al. 2014). However, there has been many controversies surrounding this topic, where other researchers suggest the possibility of asphaltenes being dissolved in crude oil (Yarranton et al. 2000; Sirota 2005). Moreover, the literature has yet to agree on the primary molecular interaction that can be held accountable for asphaltene precipitation, with one side favoring the London dispersion forces (Wiehe 2012; Redelius and Soenen 2015) whereas others signify the effect of polar bonds (Taylor 1998; Spiecker et al. 2003). Nevertheless, the presence of polar functional groups within asphaltene molecules have consistently been linked to higher polarity of asphaltenes (Moschopedis and Speight 1976b; Nalwaya et al. 1999; Wattana et al. 2005). Therefore, n-C_7 asphaltenes should have more polar functional groups than n-C_5 asphaltenes for the same crude oil. Hence, understanding how

different polar functional groups contribute to the overall polarity of asphaltenes is crucial to formulate the mechanism of asphaltene stability.

Metallo-organic compounds have consistently been discovered to reside in crude oils and asphaltenes originating from various reservoirs (Erickson et al. 1954). These trace elements naturally occur in petroleum during the formation of the source rock, where organisms and organic materials decay to form metal-rich organic layers (Barwise 1990). It is generally believed that some of these metallo-organic complexes, which can comprise of Cr, Cu, Mo, Ni, Pb, Ti, V, or Zn, are present by chelating to the porphyrin structures (McKenna et al. 2009). Most of them, however, can also exist in non-porphyrin compounds (Ali and Livingstone 1974; Fish et al. 1984). Once these metals attach onto the organic molecules, the resulting organometallic compounds have been shown to have an increase in polarity (Dunning and Rabon 1956; Fish et al. 1984; Nalwaya et al. 1999). Vanadium, in particular, was found to have a predominant role in coke formation, which is associated to asphaltene instability (Furimsky 1978; Prakoso et al. 2016). Thus, the profusion of metals in crude oils and asphaltenes can insinuate higher asphaltene polarity and instability.

Another fundamental knowledge that is necessary to describe the stability of asphaltenes in crude oil is the molecular interaction of asphaltenes with the other remaining constituents of crude oil, which can be classified as Saturates, Aromatics, and Resins (Kharrat et al. 2007; Gaspar et al. 2012). The lighter components of crude oil, which is mostly comprised of saturated hydrocarbons in the form of straight, branched, or cyclic alkanes without double or triple bonds, are identified as the saturate fraction. The

aromatic compounds, which may also contain heteroatoms such as oxygen, nitrogen, and sulfur, are classified as the aromatic fraction. Lastly, the remaining heavier portions that have similar characteristics to asphaltenes yet are more soluble in n-alkanes with higher molecular weight (e.g. n-pentane or n-heptane) are considered as the resin fraction (Speight 2006; Akbarzadeh et al. 2007). Saturates and aromatics comprise the non-polar fractions while resins and asphaltenes make up the polar fractions of crude oil (Fan and Buckley 2002).

Each fractions have different roles in establishing the thermodynamic equilibrium of the system (Rogel et al. 2012). Resins have been consistently found to have a peptizing effect on asphaltene particles in the crude oil (Carnahan et al. 1999; Lian et al. 1994; Jada and Salou 2002). Aromatic hydrocarbons, such as toluene, benzene, or xylene, are known as asphaltene dispersants. Since the aromatic fraction is primarily composed of these compounds, aromatics are generally believed to have the same dispersing effect on asphaltenes in crude oil (Jamaluddin et al. 1996; Loeber et al. 1998; Wang and Buckley 2003). In contrast, asphaltenes are observed to be insoluble in n-alkanes, which are the main constituents of saturate fraction (Wiehe et al. 2005; Akbarzadeh et al. 2005). Early studies have confirmed these findings, where crude oils with higher saturate fraction are revealed to be unstable while crude oils with higher aromatic fraction are more stable (Carbognani et al. 1999). Nonetheless, details of the interactions between these fractions and the impact they have on the overall stability of the system still require further clarification.

To evaluate the stability of asphaltenes, numerous methods have been developed over the years, which include polarity determination through dielectric constant determination (Punase et al. 2016), zeta potential measurements (Prakoso et al. 2015), onset asphaltene precipitation tests (Hammami et al. 2000), refractive index measurements (Buckley 1999), dipole moment estimations (Goual and Firoozabadi 2002), and solubility profile analysis (Rogel et al. 2010). For the first time, the contribution of various functional groups, especially for organometallic compounds, and SARA fractions towards asphaltene stability are assessed through zeta potential measurements and solubility profile analyses. Through this study, possible sources of asphaltene polarity and instability are identified. These findings would prove to be beneficial for mitigation efforts of asphaltene-related issues and enhancement of existing asphaltene precipitation models.

The goal of this study is to find a link between polarity and asphaltene stability through physicochemical characterization of the crude oil and its separated asphaltenes. Precipitating behavior of asphaltenes was also visualized with onset asphaltene precipitation tests using n-pentane, n-heptane, and the crude oil's saturate fraction as the precipitating agent. The results of these experiments provide a comprehensive insight into the variables which influence the overall stability of asphaltenes in crude oil.

CHAPTER II

RESEARCH STATEMENT

Knowledge of the molecular interactions between asphaltene and other components of crude oil (saturate, aromatic, and resin) is essential to enhance our understanding of the petroleum fluid thermodynamics. The physical and chemical properties of crude oil are primarily determined from these molecular interactions. Manipulation of these interactions can also be beneficial to reduce asphaltene-related issues and maximize the potential of a reservoir.

In this study, correlations between physical and chemical properties of crude oil are investigated to find universal, yet, simple correlations that can be used to predict asphaltenes stability. The contribution of the saturates fraction towards the overall stability of asphaltenes in crude oil is evaluated. Furthermore, the possible sources of polarity within asphaltenes and crude oils are identified and their effect on asphaltene stability is assessed.

CHAPTER III

EXPERIMENTAL PROCEDURES

The 11 different heavy oil and bitumen samples analyzed in this study come from various regions around the world, which include Canada, Colombia, Indonesia, Mexico, USA, and Venezuela. With these selection of samples, asphaltene behavior from varying original crude composition and depositional environment can be assessed to generate universal correlations. The crude oil samples were first subjected to characterization, followed by characterization on their separated asphaltenes, and finally the flocculation of asphaltene under compositional changes was simulated through onset precipitation tests.

3.1 Characterization of Crude Oils

The experiments started on density and viscosity measurements of the original crude samples. Density measurement of the samples was conducted using the Anton Paar DMA 4100 density meter at decreasing temperatures starting from 90 °C to 20 °C. The density had to be measured at higher temperatures because some of the crude were too viscous at lower temperatures, thus, restricting measurement with the density meter. However, due to the requirement described in *API MPMS* (2004) which specifies that API gravity measurements should be done under standard conditions (60 °F or 15.6 °C), previous densities found at different temperatures were extrapolated to calculate the density at standard conditions, then, this value was converted to API gravity. A similar approach was used for viscosity measurements. The Brookfield DV-III Rheometer was

used to measure viscosity at 90 ℃, then temperature was reduced till the minimum temperature values which could still provide viscosity readings. The results were then plotted and the trend line extrapolated to determine the crude oil viscosity at room temperature (22.3 ℃) to be consistent with the rest of the experimental conditions. Accuracy of the measurements were determined to be within ±0.15% °API and ±1% cP error range. From the obtained density and viscosity properties, the crude oil samples were then classified into different categories following the criteria established by the World Petroleum Council (Meyer and de Witt 1990), which acknowledges three distinct classes: heavy oil (H), extra heavy oil (EH), and bitumen (B). Crude oils with viscosity below 10,000 cP and API gravity around 10-22.3 °API are classified as Heavy oil (H). The Extra Heavy oil (EH) category is for heavier crudes which have API gravity and viscosity below 10 °API and 10,000 cP, respectively. Other samples with viscosity higher than 10,000 cP are regarded as Bitumens (B). Additionally, a special category was also created for Waxy crude oils (W) to avoid analytical errors that may be caused by the presence of hydrocarbon wax (Fuhr and Holloway 1999).

After density and viscosity measurement of the samples were completed, the bulk samples were then separated into Saturates, Aromatics, Resins, and Asphaltenes (SARA) fractions by following the *ASTM D2007-11* standard (2011). In this method, asphaltene was first separated from the bulk sample through precipitation using n-pentane. Afterwards, the deasphalted oil, also known as maltenes, was charged to a percolation chamber that contains attapulgus clay in the upper section and silica gel in the lower section. The resin fractions were adsorbed in the attapulgus clay while the aromatic

fractions were trapped in the silica gel. The unadsorbed fractions were collected below the percolation chamber and defined as the saturate fractions. During the separation and desorption process of saturates, aromatics, and resins, specific volumes of n-pentane were continuously charged into the percolation chamber to assist the flow of the fluid. A mixture of 50% toluene and 50% acetone was also used to desorb resins from the attapulgus clay. The collected fractions were then heated to 100 – 105 °C to ensure that the samples were free from contamination of the solvents. The solvents were considered to have evaporated once the weight difference within 10 minutes was less than 10 mg. Once this requirement was achieved, the weight fractions were recorded and the remaining weight fraction was assigned to the aromatic fractions.

To provide accurate comparisons with n-pentane asphaltenes as well as minimize solvent and time consumption, the n-heptane asphaltenes were taken from the OAP test results which used the same ratio of 10 mL of solvent / g of oil and followed similar filtration procedure as ASTM D2007-11 (Buenrostro-Gonzalez et al. 2004). The amount of n-heptane insoluble obtained from this experiment have been checked to be similar to the ones produced from other ASTM method, i.e. *ASTM D3279-12* (2012a). The procedure details for n-heptane separation is elaborated more in the OAP test section.

Chemical characterization of the crude samples include Fourier Transform InfraRed (FTIR) spectroscopy using the Agilent Cary 630 Attenuated Total Reflection (ATR) spectrometer. The analyses of FTIR spectra are complex, hence, the obtained FTIR spectra were compared with the FTIR spectra of reference samples; such as attapulgus clay, silica gel, acetone, toluene, n-pentane, n-heptane and distilled water.

Elemental analyses were conducted by Chevron on both the crude oil and the n-pentane asphaltene to assist in the detection of polar functionalities within the samples (Rogel, Roye, et al. 2015). Standard combustion method, using a Leco CHN analyzer Carlo Erba model was used to estimate the carbon, hydrogen, and nitrogen content in the test sample. A Thermo Intrepid Inductively Coupled Plasma was then used to measure the composition of the trace elements.

To assess asphaltene stability in crude oils, Solubility Profile Analysis was conducted by Chevron using their in-house High Performance Liquid Chromatography (HPLC) system which consisted of a HP Series 1100 chromatograph and an Alltech Evaporative Light Scattering Detector (ELSD) 2000. To begin the experiment, the crude samples were first mixed with dichloromethane. The resulting solution was then injected into the HPLC column together with n-heptane which acted as the mobile phase. After all of the n-heptane solubles (maltenes) have eluted from the column, the mobile phase was gradually changed to 90:10 dichloromethane/methanol and then to 100% methanol (Rogel et al. 2010). The ELSD was then used to quantify the amount of asphaltenes precipitated and generate the solubility curve. From the solubility curve, the stability parameter known as ΔPS was then calculated from the time difference between 75% and 25% elution of the material (Rogel et al. 2010).

3.2 Characterization of Asphaltenes

Three methods were used to determine asphaltene content of crude oils; ASTM D2007-11 in which nC_5 was used as the precipitating agent, ASTM D6560-12 and the on-

column precipitation from the HPLC experiment which used nC_7 to separate the asphaltenes. Physical characterization of asphaltenes then include: i- visual inspection, ii- optical microscopic imaging, iii- SEM imaging for surface morphology, iv- density measurements, v- cluster size determination by particle size analyzer. All of these analyzes were conducted for both nC_5 and nC_7 asphaltenes. It is important to note, however, that asphaltenes determined from the HPLC method was consumed, rendering it unavailable for further analysis.

Asphaltene density measurements followed the procedure developed by Barrera et al. (2013) which calculates the density from asphaltene-toluene mixtures. Varying amounts of asphaltenes were first prepared and mixed with a constant volume of toluene to produce solutions with different asphaltene weight fractions. The mixture density was then measured using the Anton Paar DMA 4100 density meter at room temperature and the specific volume of mixture calculated (inverse of density). A plot of specific mixture volume vs asphaltene weight fraction would then generate the slope and intercept value which will be used in simple mixture density calculations to estimate the density of asphaltene.

Then, nC_5 and nC_7 asphaltenes were subjected to zeta potential and cluster size analyses. The Brookhaven Instruments Corporation ZetaPALS Zeta Potential Analyzer and 90 Plus Particle Size Analyzer were used to measure zeta potential and cluster size, respectively. Zeta potential is a measure of electrostatic repulsion between colloidal particles, which is known to affect colloidal stability (Jada and Salou 2002). Hence, zeta potential measurements can provide definitive information regarding polarity of

asphaltenes. Both zeta potential and cluster size measurements were conducted on the same solutions that were prepared by following the procedure reported by Parra-Barraza et al. (2003). Accordingly, 50 mg of asphaltenes was added into 15 mL of ethanol and sonicated in an ultrasound tub for 20 minutes to homogenize the dispersion of asphaltenes. 1.5 mL of this solution was then mixed with 100 mL of 1 mM KCl (Parra-Barraza et al. 2003). 1 mM KCl solution was selected as the dispersion medium due to its low ionic strength which can minimize the effect of the dispersion medium on zeta potential measurements (Wiącek and Chibowski 1999; Salgın et al. 2012). The same solutions were used to measure the total dissolved solids (TDS) and pH value with the Oakton TDS and pH meter.

The asphaltene samples were further analyzed under different microscopy techniques. The optical microscopy observation was conducted using the Meiji Techno Microscope equipped with Jenoptik ProgRes CT5 camera under 100X magnification. Another microscopic imaging technique used in this study is the SEM-EDS. The Tescan Vega 3 microscope was used to examine the surface chemistry and morphology of the asphaltene samples. Furthermore, the Digital Instruments MultiMode AFM microscope was also tested to assess the particle size of asphaltenes when dispersed in toluene.

Asphaltene samples were analyzed using the Agilent Cary 630 Attenuated Total Reflection (ATR) spectrometer for the same purposes as FTIR analysis of crude oil. First, the obtained FTIR spectra were compared with the FTIR spectra of reference samples, such as distilled water, n-pentane, n-heptane, toluene, acetone, silica gel, and attapulgus clay, to detect traces of contamination or presence of water or wax in the samples.

3.3 Onset Asphaltene Precipitation (OAP) Test

To mimic the alteration in crude oil composition during production, the bulk samples were mixed with n-pentane, n-heptane, or the crude oil's own saturate fraction (Buenrostro-Gonzalez et al. 2004). 5 g of oil is mixed with varying concentrations of solvent ratio (mL of solvent / g of oil), starting from 1 mL/g to 30 mL/g. The solution is then homogenized in an ultrasound tub for 15 minutes and left to equilibrate for 24 hours. Subsequently, the solution is charged through a 0.45 microns filter paper using the filtration assembly. The unfiltered fractions are then heated inside the vacuum oven for at least 24 hours to ensure the evaporation of the solvents and the remaining weight is measured. The ratio of asphaltene weight to original weight of the sample is then taken as the weight fraction of the precipitated asphaltenes.

For the OAP test using the saturates fraction, similar procedures were followed but at lower concentrations of solvent ratio. This is due to the difficulties associated with the procurement of saturates from the SARA separation of the bulk samples, since the ASTM D2007-11 method only produces small amounts of saturates (maximum 3 g of saturates out of 10 g of oil). Hence, only solvent ratios of 1, 3, and 5 ml/g were feasible for these tests.

CHAPTER IV

EXPERIMENTAL RESULTS*

4.1 Characterization of Crude Oil and Bitumen Samples

The results from viscosity and density measurements of the 11 different bitumen and crude oil samples are listed below in **Table 1**. The crude oils were then categorized based on their physical properties following the criteria established by the World Petroleum Congress (Meyer and de Witt 1990). Crude oils with viscosity below 10,000 cP and API gravity around 10-22.3 °API are classified as Heavy oil (H). The Extra Heavy oil (EH) category is for heavier crudes which have API gravity and viscosity below 10 °API and 10,000 cP, respectively. Other samples with viscosity higher than 10,000 cP are regarded as Bitumens (B). Additionally, a special category was also created for Waxy crude oils (W) to avoid analytical errors that may be caused by the presence of hydrocarbon wax (Fuhr and Holloway 1999).

* Reprinted with permission from "A Mechanistic Understanding of Asphaltene Precipitation from Varying Saturate Concentration Perspective" by Prakoso, A.A., Punase, A.D., Hascakir, B., 2015. Presented at SPE Latin American and Carribean Petroleum Engineering Conference, Quito, Ecuador, 18-20 November. Copyright 2016 by Society of Petroleum Engineers.

Table 1: Physical properties and SARA fractions of 11 crude oils. API gravity is measured at standard temperature (60 °F) while other measurements are taken at room temperature (22.3 °C).

Sample	API Gravity (°API)	Viscosity (cP)	Saturates* (wt%)	Aromatics* (wt%)	Resins* (wt%)	nC_5 Asph.* (wt%)	nC_7 Asph.** (wt%)	nC_5:nC_7 Ratio
H1†	17.12	496	30.03	41.84	15.56	12.57	1.72	7.31
H2	12.19	167660	11.01	44.89	20.75	23.35	11.15	2.09
H3	18.84	884	22.63	37.57	16.03	23.76	5.71	4.16
H4†	12.56	263273	32.02	21.95	7.95	38.08	8.26	4.61
EH1	7.97	251083	12.70	42.11	22.93	22.26	13.40	1.66
EH2	11.56	208585	10.14	38.01	13.09	38.76	21.42	1.81
B1	12.09	10139	16.51	37.81	17.10	28.58	9.90	2.89
B2†	8.19	53146	23.60	20.00	21.90	34.30	30.41	1.13
B3	6.11	12050473	10.68	29.10	20.14	40.08	21.27	1.88
B4	10.01	19196251	11.05	30.47	16.06	42.41	37.74	1.12
W1	27.05	676	24.28	25.00	5.43	45.30	9.90	4.58

*Based on ASTM D2007-11

**Based on results from 10 mL/g solvent ratio (Buenrostro-Gonzalez et al. 2004)

H, EH, B, and W correspond to the classification of crude oil: Heavy oil, Extra Heavy oil, Bitumen, and Waxy crude oil, respectively.

†Samples contain water.

From a quick glance, we can see that API gravity and viscosity do not show direct correlation. Hence, the popular preconception that heavier oil would lead to a more viscous oil is proven to be not valid for all crude oils. However, there should still be an indirect relationship between viscosity and API gravity, which will be investigated in later sections.

After physical properties of the bulk samples have been measured, composition of the crude oils were then quantified. The SARA weight fractions for all samples are also included in Table 1. When physical properties of the bulk samples are compared with their SARA fractions, some correlations between the dataset can be found. The weight percent

of saturate fraction is found to have weak linear relationship with API gravity and inverse exponential correlation with viscosity. The opposite trends are observed for the resin and asphaltene weight fractions, where increasing weight percent is followed by decreasing API gravity and increasing viscosity.

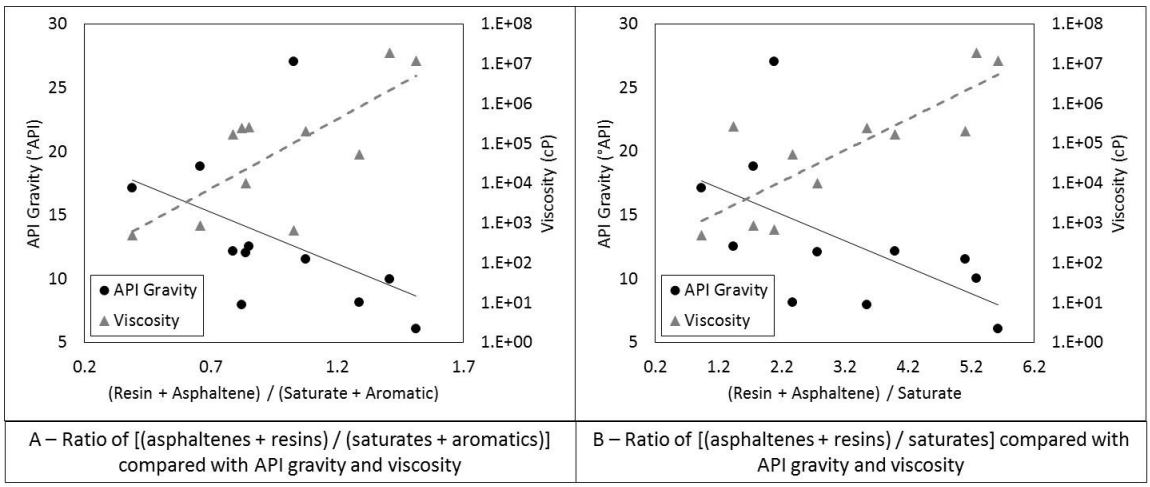

A – Ratio of [(asphaltenes + resins) / (saturates + aromatics)] compared with API gravity and viscosity

B – Ratio of [(asphaltenes + resins) / saturates] compared with API gravity and viscosity

Figure 1: Correlation of heavy-to-light fractions of crude oil to API gravity and viscosity (Heavy: Asphaltenes and Resins; Light: Aromatics and Saturates)

From these correlations we can conclude that higher concentration of heavier molecules have a tendency to increase density and viscosity of crude oil. To further test this hypothesis, we looked into the comparison of physical properties with compositional ratios of heavy-to-light fractions [(ASP+RES)/(ARO+SAT)]. In **Figure 1**, the two of such ratios are compared with density and viscosity of the sample. The results have exhibit trends which agree to our previous hypothesis. Therefore, heavy molecules within crude oils play an important role in the determination of crude oil's physical properties, though, their interactions with light fractions can also surpass their impact on API gravity and viscosity of the bulk oil.

Nevertheless, some outliers are still noticeable within the dataset. Even though SARA fractionation have helped to simplify the characterization process of the diverse components of crude oil (McCain 1990), it is clear that information obtained solely from weight percent of SARA fractions is still not sufficient to fully describe the complex molecular interactions occurring within the crude oil. Hence, chemical characterization on the crude samples through FTIR analysis is required to gain further insight on these molecular-scale mechanisms.

FTIR spectroscopy is a powerful tool which can be used to determine physicochemical properties of crude oil such as asphaltene content and viscosity (Wilt et al. 1998; Sastry et al. 1998; Li et al. 2012). Analysis of FTIR spectroscopy provide valuable information regarding the molecular structure and bonds which exists within the sample. To interpret FTIR curves, the observed peaks are connected to the corresponding molecular bonds and the combination of these bonds are then construed to describe the molecular formulation of the sample. For hydrocarbon molecules, $–CH_3$ groups exhibit a significant peak around 2953 cm^{-1} wavenumber while $–CH_2$ bonds are shown by the peak at 2853 cm^{-1} (Benkhedda et al. 1992). Significant peaks in the range of 1475, 1450, and 1375 cm^{-1} are associated with bending vibrations of methylene and methyl groups (Wilt et al. 1998). Aromatic C–H bonds appear at the shoulder peak around 3100-3000 cm^{-1} while the in-plane and out-of-plane bending are represented by peaks in the 1300-1000 and 900-675 cm^{-1} wavenumber regions, respectively (Sastry et al. 1998). Additionally, aromatic compounds would also display a peak at 1600 cm^{-1} which are linked to C=C bonds (Bellamy 1980).

In this study, determination of functional groups within the crude oil components are of particular interest because of their effect on the overall polarity and stability of the system. Hydrogen bonds (e.g. O–H or N–H bonds) are shown by a stretched peak in the wavenumber range of 3600-3100 cm^{-1} (Castro and Vazquez 2009; Moschopedis and Speight 1976a). Oxygen functional groups, such as esters, ketones, aldehydes, carboxylic acids, and carbonyls are found within the 1735-1650 cm^{-1} regions (Calemma et al. 1995; Kar et al. 2014). Another type of heteroatoms often found in crude oils are sulfurs, which are generally in the form of sulfoxides (1030 cm^{-1}), aliphatic sulfides, thiols (2600-2400 cm^{-1}), and thiopenes (Green et al. 1993). Moreover, nitrogen functional groups also exist as pyrroles, pyridines, indoles, and carbazoles, where –NH and C–N bonds may appear at around 3600-3100 cm^{-1} and 1300-1100 cm^{-1} respectively (Snyder et al. 1968; Larkin 2011).

One example is provided in **Figure 2** to explain how FTIR spectra can be analyzed. Four crude oils from different categories were selected, which are samples H1, EH2, B3, and W1, shown in black, red, green, and blue lines, respectively. FTIR spectra for the rest of the samples are given in **Figure A-1**.

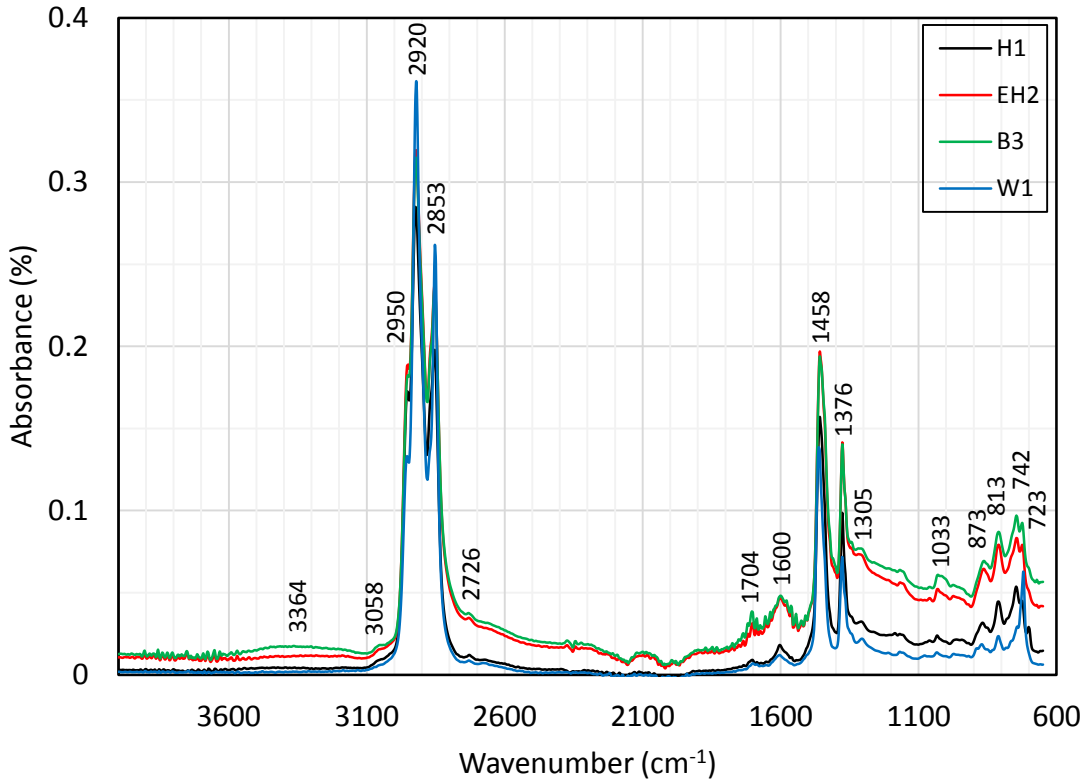

Figure 2: FTIR spectra of 4 different types of crude oil. Other FTIR spectra can be found in the appendix section (Figure A-1).

As observed in Figure 2, these crude oils are primarily dominated by hydrocarbon chains (mostly aliphatic and aromatic) but also show hints of specific functional groups in the fingerprint region. Aside from the C–H groups that are shown in 2950-2853 cm^{-1} and 1458-1376 cm^{-1} wavenumbers, other functional groups that seem predominant in crude oil are hydrogen bonds (3364 cm^{-1}), carbonyl groups (1704 cm^{-1} and 1305 cm^{-1}), and sulfur groups (1033 cm^{-1}) (Moschopedis and Speight 1976a; Siddiqui and Ali 1999; Wilt et al. 1998). However, multiple molecular groups have overlapping peaks within these wavenumber regions, which further complicate the distinction of specific functional groups in the crude oil without other complementary techniques (Siddiqui and Ali 1999).

It is also important to note that the peaks in the 2300-1800 cm^{-1} can be disregarded due to a noise caused by the ATR diamond crystal (Unur 2013).

When four spectra of different types of crude oils are compared, their FTIR spectra exhibit a lot of similarities with each other. However, it can be discerned that the heavier crudes and bitumens display higher absorbance values in the aromatic and functional groups wavenumber regions compared to their lighter counterparts. This trend suggests that heavier crudes and bitumens are more aromatic and contain larger amounts of heteroatoms, which is the cause for heavier and more viscous nature of the crude oil. Additionally, an anomaly was observed for the FTIR spectrum of sample W1 in the $(CH_2)_n$, n>4 bond region shown by the tall peak at 722 cm^{-1}, which represents very long aliphatic hydrocarbon chains and has previously been connected to the signature of hydrocarbon wax (Musser and Kilpatrick 1998; Krump et al. 2005).

To further understand the chemical composition of the crude oil, elemental analyses were carried out by Chevron and the results were listed in **Table 2**. The analysis have indicated the presence of N, O, S, and other metallic (inorganic) elements within the crude oil. Hence, the functional groups identified through the FTIR spectra have been verified to exist, with oxygen groups being the most abundant followed by sulfur and nitrogen functional groups, respectively. Note that oxygen amount was calculated by the remaining wt%, thus, it may also include other elements that are not detected by the machine, mainly anions such as Cl.

The elemental composition of crude oils can give significant clues on the molecular structure of the crude oil and the inorganic content of the reservoir rock host

the crude oil. For example, nickel (Ni) and vanadium (V) are common organometallic content of crude oils; however, other metals, such as calcium (Ca), iron (Fe), magnesium (Mg), potassium (K), sulfur (S), nickel (Ni), and sodium (Na), are known to originate from the reservoir rocks and/or brine (Groen and Craig 1994; Bennett et al. 1993). For instance, crude oil B4 has the highest amount of calcium and magnesium. This crude oil is most likely produced from a carbonate reservoir, which consists of mainly calcite ($CaCO_3$) and dolomite ($CaMg(CO_3)_2$). Crude oil B2 shows similar patterns due to the fact that it comes from a Canadian oil sands reservoir, which is known to have sections of carbonate formations (Bayliss and Levinson 1976). Sample EH2 has high amounts of iron and sulfur, which may come from iron-rich sediments containing large amount of pyrite (FeS_2). Similarly, the high concentration of iron in H2 and H4 crude oils, which are produced from sandstone reservoirs, may come from the hematite and magnetite minerals. Additionally, crude oils B3, B4, and B2 contain appreciable amounts of potassium, an indication of high clay content (Weaver 1967), which may come from shale layers found throughout the reservoirs (Takahashi and Torigoe 2008; Bayliss and Levinson 1976). These samples also have high sodium content, which is most likely due to brine from the shales. Furthermore, sulfur can constantly be seen as the largest source of heteroatoms among the crude oil samples. Sulfur can exist in either organic or inorganic compounds, such as thiols, sulfides, thiophenes, and pyrites (Manahan 1990; Waldo et al. 1991). From these analyses, it is clear that the crude oils analyzed in this study have both organic and inorganic contents.

Table 2: Elemental analysis of crude oil

Crude oil composition											
Elements, wt%	**H1†**	**H2**	**H3**	**H4†**	**EH1**	**EH2**	**B1**	**B2†**	**B3**	**B4**	**W1**
C	81.3	80.9	81	72.91	83.5	80.6	80.9	80.3	81.2	80.8	84.4
H	11.5	11	11	10.53	10.6	10.5	10.8	10.3	10.4	10.3	13.4
H/C	1.70	1.63	1.63	1.73	1.52	1.56	1.60	1.54	1.54	1.53	1.91
O*	2.99	4.45	5.55	14.71	1.24	2.53	2.86	1.46	1.48	1.56	1.08
N	≤1	1.26	≤1	≤1	≤1	≤1	≤1	≤1	≤1	≤1	≤1
S	3.2	2.35	1.43	0.81	3.6	5.24	4.41	6.87	5.82	6.22	0.119
Heteroatoms**	7.2	8.1	8	16.56	5.9	8.9	8.3	9.4	8.4	8.9	2.2
Trace elements, ppm											
Al	1.2	2.35	n.d.	n.d.	n.d.	n.d.	n.d.	n.d.	n.d.	n.d.	n.d.
B	9.41	14.6	4.02	20.5	1.87	1.59	2.68	22.8	18.1	3.32	n.d.
Ca	6.96	14.4	7.14	1.5	2.5	n.d.	n.d.	84.1	10.2	291	n.d.
Cu	1.77	n.d.	n.d.	n.d.	n.d.	n.d.	n.d.	n.d.	n.d.	n.d.	n.d.
Fe	6.4	80.3	6.82	147	3.68	224	2.49	14.6	31.9	5	n.d.
K	5.1	5.1	5	6	5.7	5.2	5.8	23	13	42	5.1
Mg	12.4	2.73	2.08	1.2	n.d.	n.d.	n.d.	5.11	n.d.	20.3	n.d.
Mo	n.d.	2.41	n.d.	n.d.	1.4	475	8.9	7.82	14.6	11.4	n.d.
Na	21.5	67	74.5	17	58.1	8.46	23.3	235	504	209	14.8
Ni	4.31	78.4	20	20.9	95.3	88.4	68.1	80.3	9.76	100	7.46
P	2.1	2.1	2	2.4	2.3	2.1	2.4	2	2.1	2.2	2.1
Pb	n.d.	2	n.d.	n.d.	n.d.	n.d.	n.d.	n.d.	n.d.	n.d.	n.d.
Si	3.49	11.4	n.d.	112	n.d.	45.1	n.d.	7.49	131	2.7	n.d.
Sn	n.d.	1.4	n.d.	1.2	n.d.	1.4	1.2	1.5	n.d.	n.d.	n.d.
Ti	n.d.	4.22	n.d.	n.d.	2.68	n.d.	2.94	3.18	3.9	n.d.	n.d.
V	10.4	110	38.8	77.3	402	469	172	218	258	512	n.d.
Zn	n.d.	1.1	n.d.	1.2	4.09	n.d.	n.d.	5	n.d.	n.d.	n.d.
Metals***	70	371	154	273	575	1271	285	678	845	1191	27

*O is calculated from the remaining wt%

**Heteroatoms is the sum of all elements and trace elements (in wt%) except for C and H

***Metals (in ppm) is the sum of all metallic elements (i.e. Al, Ca, Cr, Cu, Fe, K, Mg, Mo, Na, Ni, Pb, Sn, Ti, V, and Zn)

†Samples contain water.

To determine the effect of heteroatoms on the physicochemical characteristics of crude oil and bitumens, elemental values of the samples were compared with the physical properties of crude oil (Table 1) using correlation plots in **Figure 3**. Accordingly, Figure 3-A, 3-B, 3-C, and 3-D provide the relationship of heteroatom content with respect to API gravity, viscosity, n-pentane and n-heptane asphaltene content.

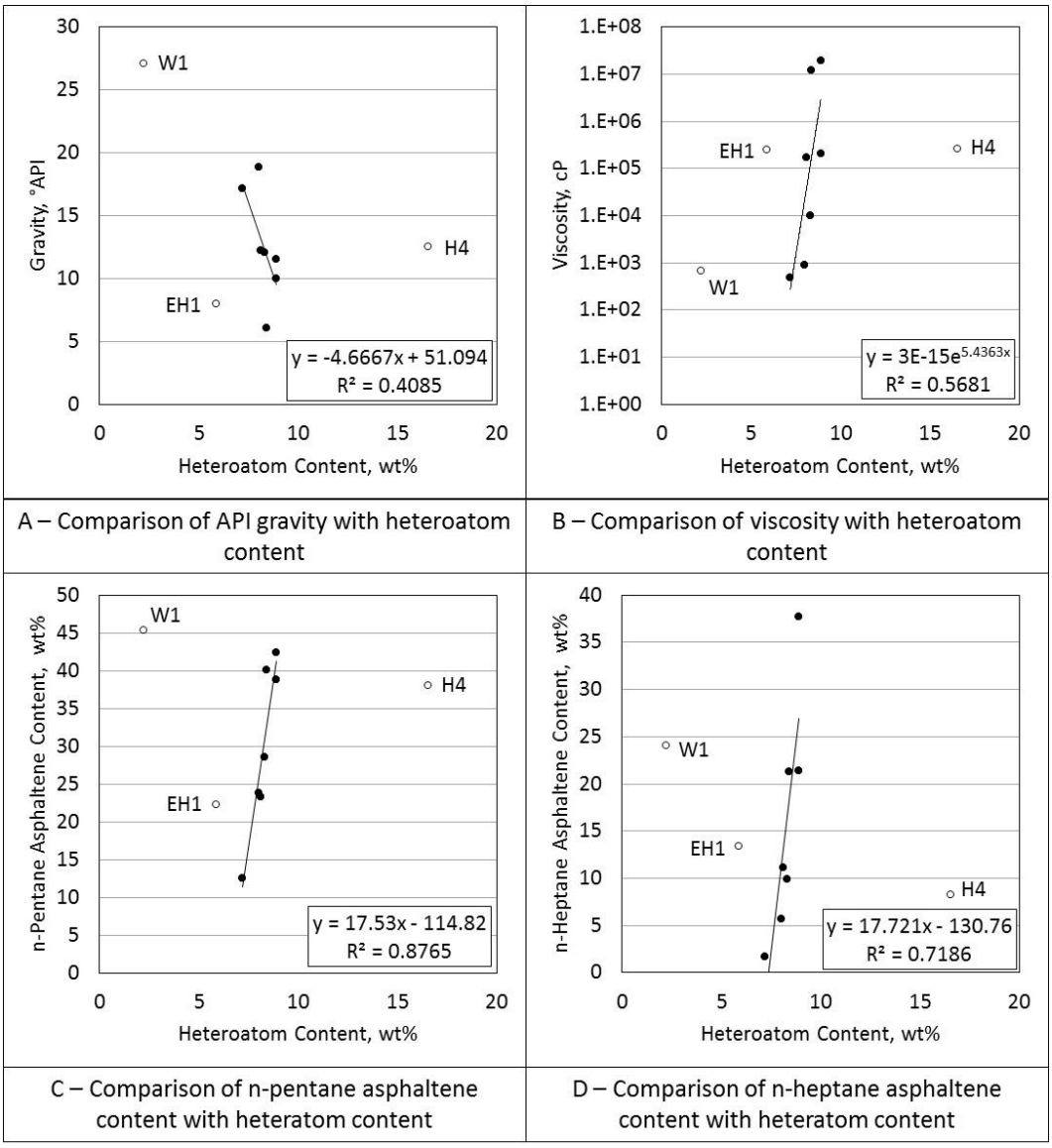

Figure 3: Correlations of heteroatom content (Table 2) with physical properties of crude oil (Table 1). Blank circles represent outliers in the dataset.

The outliers in each dataset are shown as blank circles while data points that are in good agreement with the trend are represented by the black dots. Contribution of the outliers were excluded from the correlations given in each figure. Though linear relations

were provided in the graph, Figure 3-C and 3-D also exhibited good exponential correlations (R^2 value of 0.9242 and 0.9196).

Correlations in Figure 3 show that crude oils and bitumens with higher concentration of heteroatoms will be heavier, more viscous, and contain more asphaltenes. This trend agrees with the FTIR spectra, where the heavier and more viscous samples show higher peaks in the wavenumber regions for heteroatom functional groups. Nevertheless, the dataset contain some anomalies for sample H4, EH1, and W1. Sample H4 have abnormally higher concentration of non-hydrocarbon elements compared to the other samples while the opposite holds true for sample EH1. Sample W1 has a fundamental difference in chemical composition caused by the presence of hydrocarbon waxes (Fuhr and Holloway 1999).

To isolate the elements which have the most impact on the physicochemical constitution of crude oil, each elemental group are analyzed in the same manner as the heteroatoms. From assessment on the organic components, sulfur content seem to have the best correlation with physical characteristics of the crude oil as displayed in **Figure 4**. The correlation plots revealed that sulfur contributes to the increase in density, viscosity, and asphaltene content of crude oil. Oxygen, to a lesser extent, also show similar trends but not for nitrogen.

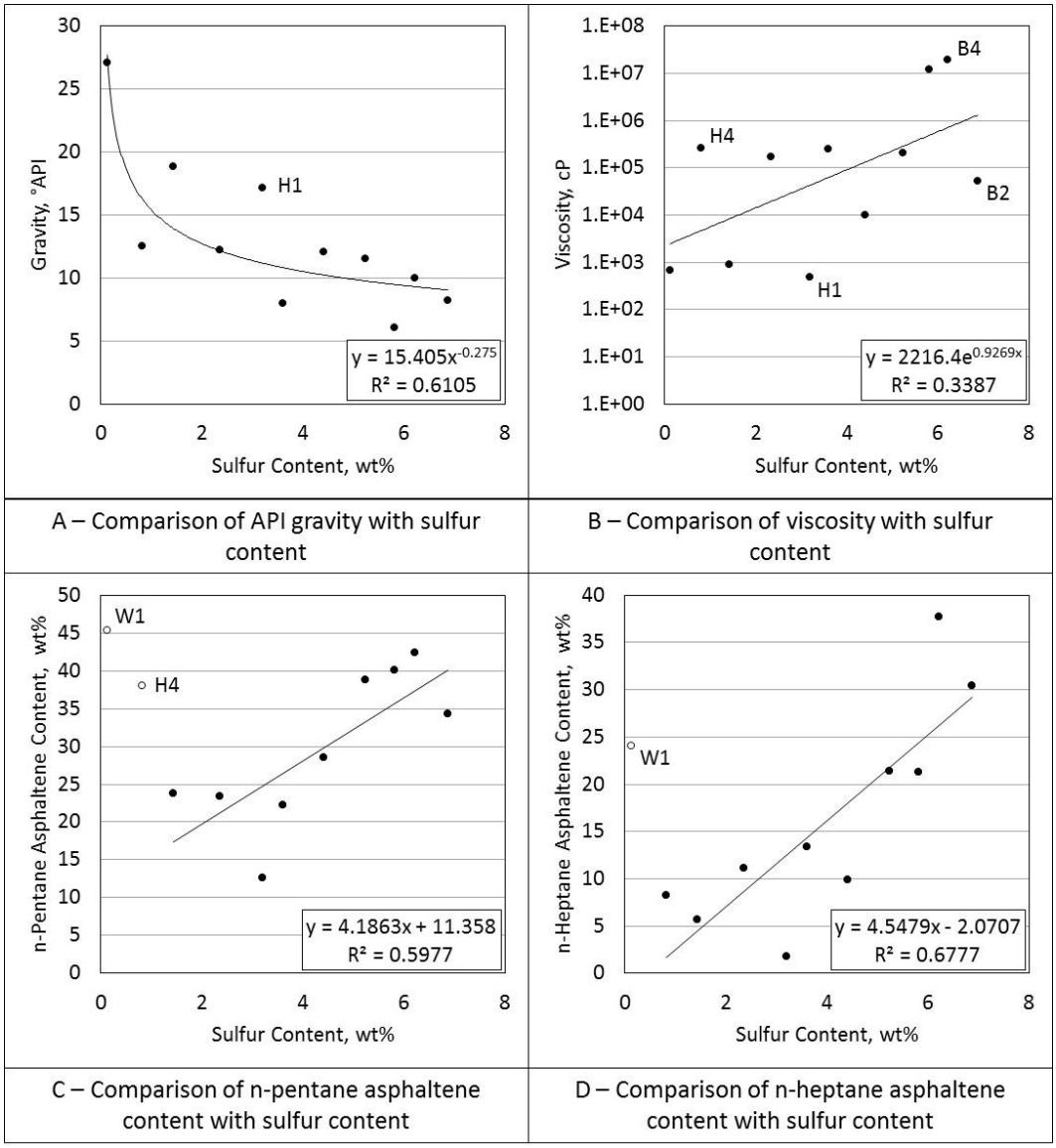

Figure 4: Correlations of sulfur content (Table 2) with physical properties of crude oil (Table 1). Blank circles represent outliers in the dataset.

Another elemental group which show great relationship with physical parameters of crude oil is the metallic constituents. In **Figure 5**, the concentration of metals in the crude oil is revealed to correlate well with API gravity, viscosity, and asphaltene content of the bulk samples. Therefore, even though these inorganic elements make up only a very

small portion of the crude oil, they still have a large influence in determining the physical properties of the crude oils and bitumens. Unfortunately, the presence of these trace elements cannot be detected through FTIR spectroscopy due to the limitations of the ATR spectrometer (Chan and Kazarian 2006).

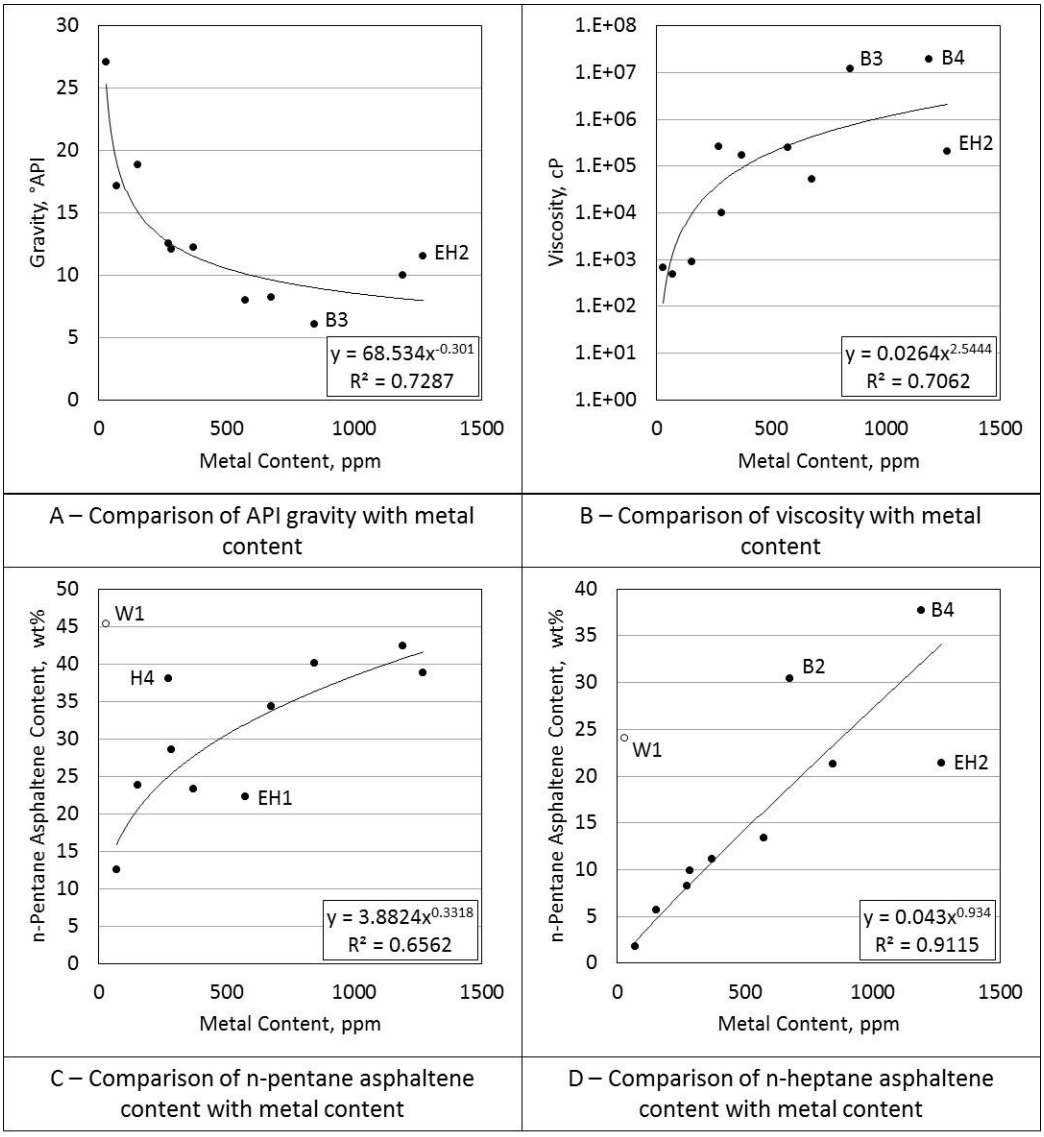

Figure 5: Correlations of metals content (Table 2) with physical properties of crude oil (Table 1). Blank circles represent outliers in the dataset. (Metals detected: Al, Ca, Cr, Cu, Fe, K, Mg, Mo, Na, Ni, Pb, Sn, Ti, V, and Zn).

Evaluation of the solubility profile of asphaltenes can provide additional insight into the colloidal stability of crude oils (Rogel et al. 2010). Varying solubility profile distributions can be observed on crude oils from different origins as seen in **Figure 6** and **Figure A-3**. The black, red, green, and blue curves represent solubility profile of sample H1, EH2, B3, and W1, respectively.

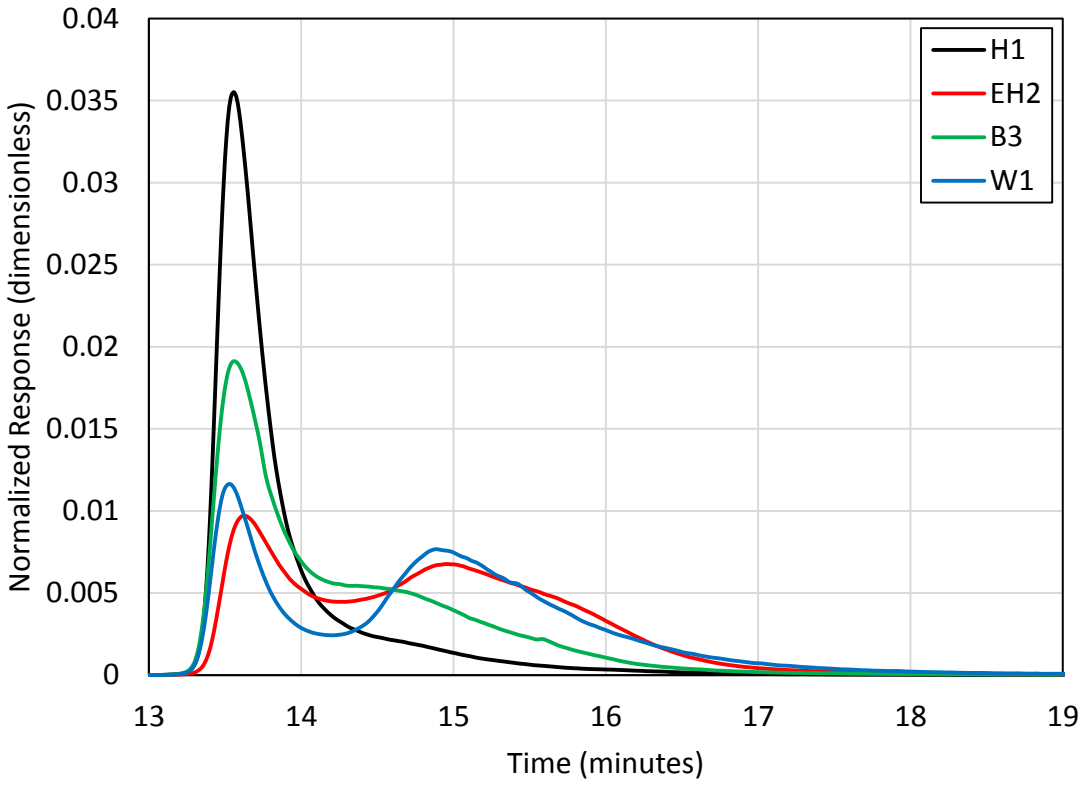

Figure 6: Solubility profile of 4 different types of crude oil. The solubility profiles for other crude oil samples are listed in Figure A-3.

Looking at the curves in Figure 6 and A-3, two distinct distribution of asphaltene solubility profile are observed: unimodal and bimodal. In terms of asphaltenes stability, the unimodal distribution represents higher stability compared to the bimodal distribution

(Rogel et al. 2010). Two or more peaks within the solubility profile indicate that molecular compounds within the sample have varying solubility, which can imply immiscibility between the components, hence, higher risk of precipitation (Rogel et al. 2010, 2012). From this definition, samples with bimodal and wider distribution can then be regarded as less stable compared to their counterparts. To help relate the shape of the distribution with stability, a quantifiable parameter ΔPS is created. ΔPS values for each sample were calculated from the solubility profiles using **Equation 1** (in Appendix) and listed in **Table 3**. Accordingly, samples with higher ΔPS value is found to be less stable and are more prone to precipitation (Rogel et al. 2010).

Table 3: ΔPS values for 11 crude oil samples

Sample	ΔPS
H1†	0.40
H2	1.25
H3	1.04
H4†	2.02
EH1	1.79
EH2	1.83
B1	1.36
B2†	1.24
B3	1.17
B4	0.63
W1	1.99

†Samples contain water.

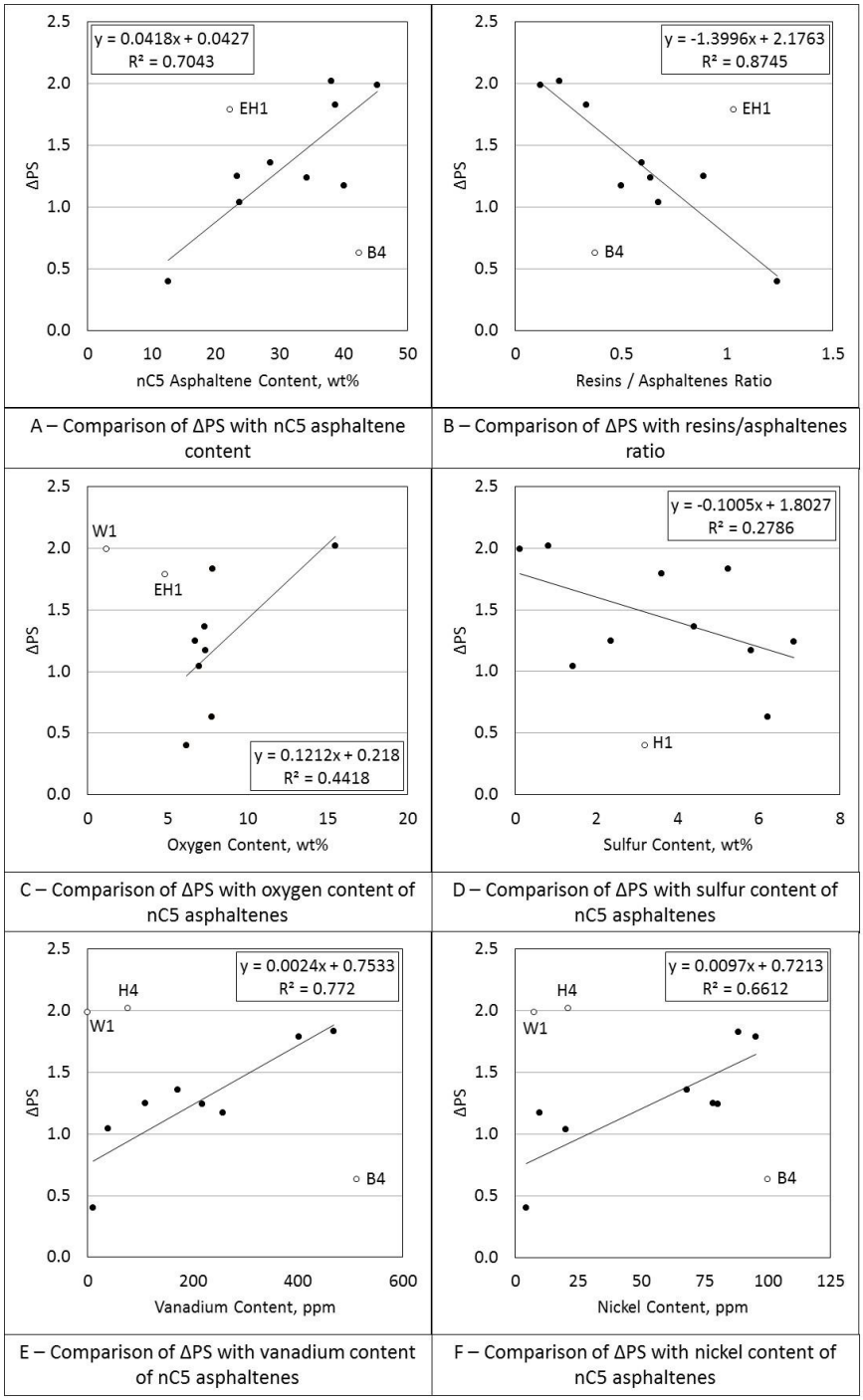

Figure 7: Correlations of ΔPS parameter (Table 3) with SARA (Table 1) and elemental compositions (Table 2) of crude oil. Blank circles represent outliers in the dataset.

The values in Table 3 were then correlated to SARA fractions (Table 1) and elemental compositions of crude oil (Table 2). From correlation plots in **Figure 7**, it can be observed that both SARA fractions and elemental compositions of crude oil have a large influence on the colloidal stability of crude oils.

Figure 7A displays how increasing asphaltene concentration can negatively affect stability of crude oil. However, the presence of resins within the crude oil also need to be accounted for, because they have a significant contribution toward stabilizing asphaltenes within the crude oil, as seen in Figure 7B. Heteroatoms such as oxygen and sulfur in the form of different functional groups may affect the stability of asphaltenes (Figure 7C and 7D). Furthermore, vanadium and nickel play a vital role in destabilizing asphaltenes (Figure 7E and 7F), even though their concentration within the crude oil are miniscule compared to the major heteroatoms (N, O, S).

4.2 Characterization of Asphaltenes

Asphaltene characterization were carried out in a similar approach that was applied to the crude oil samples. Since there is no unique definition of asphaltenes, characterization studies for asphaltenes were conducted on asphaltenes separated from three different methods. In the literature, separation of asphaltenes using n-heptane (nC_7) have been found to isolate heavier and more polar materials from the crude oil compared to n-pentane (nC_5) separation (Ortega et al. 2015; Barrera et al. 2013). However, as seen in **Table 4**, the density of nC_7 asphaltenes are not always higher than nC_5 asphaltenes. This trend is also seen across the four different class of crude oil, not only for a specific

class of crude oil. Our results suggest that more polar part of the asphaltenes are not always denser than the less polar part of asphaltenes.

Table 4: Asphaltene densities in g/cc. Calculation and measurement methods are based on the procedure developed by Barrera et al. (2013).

Sample	nC_5 Asphaltene Density	nC_7 Asphaltene Density
H1†	1.21	1.10
H2	1.16	1.12
H3	1.16	1.21
H4†	1.08	1.20
EH1	1.18	1.16
EH2	1.16	1.17
B1	1.28	1.12
B2†	1.05	1.16
B3	1.12	1.44
B4	1.15	1.17
W1	0.95	0.89

†Samples contain water.

When densities of both n-pentane and n-heptane asphaltenes (Table 4) are correlated with physical properties of crude oil (Table 1) in **Figure 8**, asphaltene density is shown to directly relate with density and viscosity of crude oils. This finding purports the logic that denser materials would contribute to higher crude density and viscosity. Thus, the heavy constituents of crude oil can be regarded as the dominant components in shaping the physical properties of crude oil.

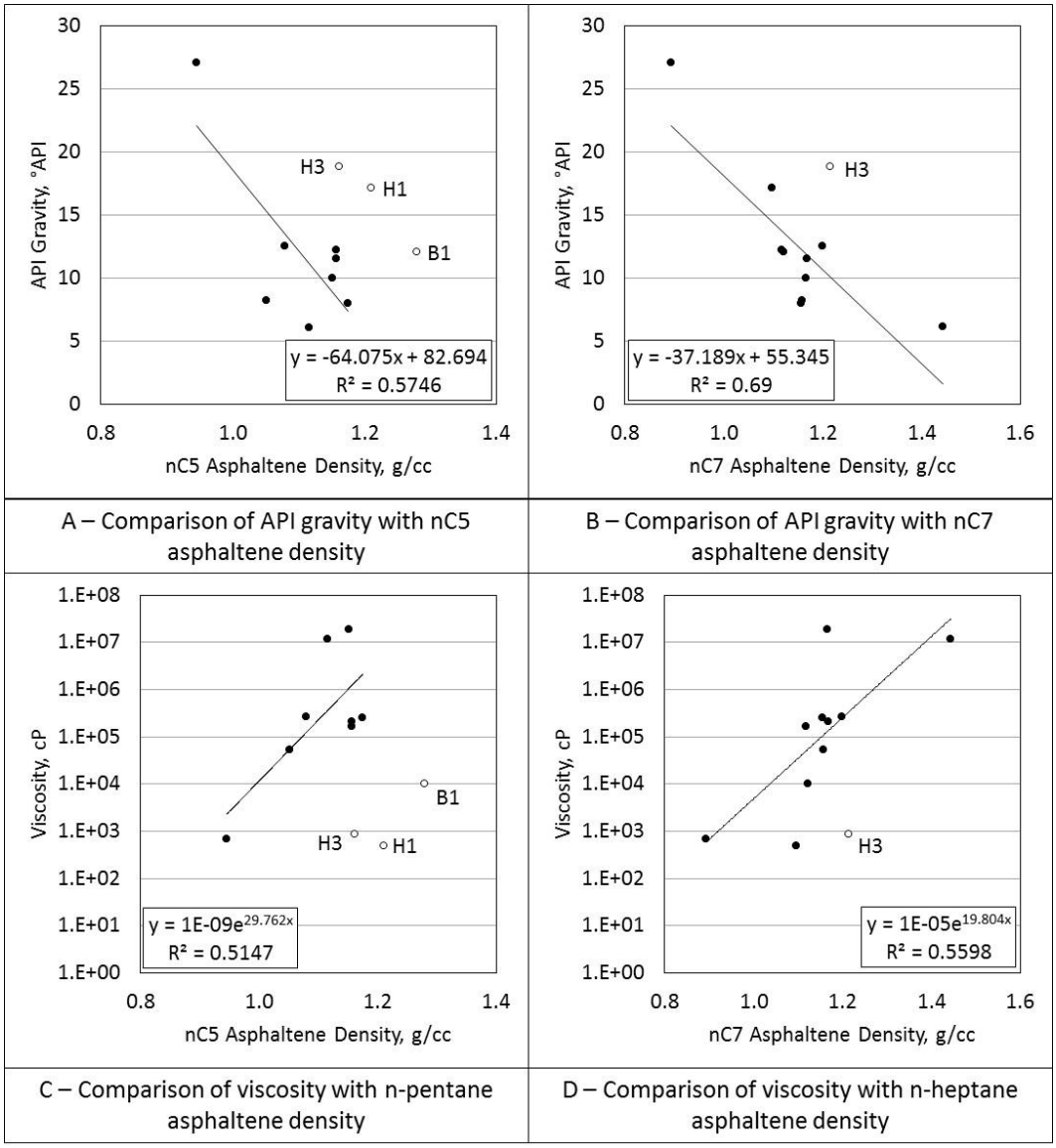

Figure 8: Correlations of asphaltene density (Table 4) with physical properties of crude oil (Table 1). Blank circles represent outliers in the dataset.

Molecular assessment of the asphaltene samples is necessary to distinguish the polar functional groups that are responsible for the stability of asphaltenes within the crude oil. A similar approach is taken to analyze these properties, where FTIR spectroscopy and elemental analysis are utilized to isolate functional groups of interest. A comparison of

FTIR spectra between original crude oil and the separated n-pentane and n-heptane asphaltenes are provided for sample EH2 in **Figure 9**. The red, black, and grey lines each represent FTIR spectrum of the crude oil, n-pentane asphaltenes, and n-heptane asphaltenes, respectively. FTIR spectra for other samples are included in **Figure A-1**.

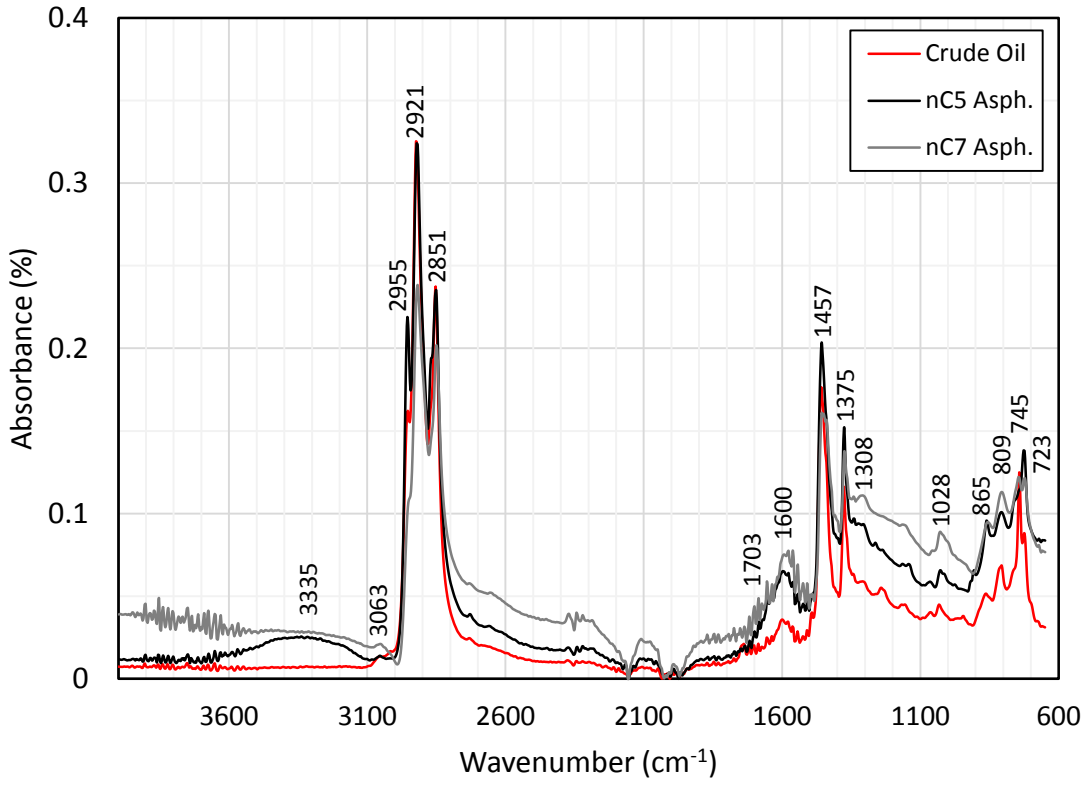

Figure 9: FTIR spectra of original crude oil, n-pentane and n-heptane asphaltenes of sample EH2

Previous studies have concluded that FTIR spectra of n-pentane and n-heptane asphaltenes exhibit similar molecular structures and undistinguishable features (Nalwaya et al. 1999). Observation from Figure 9 show that the overall spectra of n-pentane and n-heptane asphaltenes are similar, though, the intensity of the absorbance peaks are different

in several wavenumber regions. For instance, in the hydrogen bond region n-pentane asphaltene is shown to have larger peak than n-heptane asphaltene. This finding agrees with the literature where abundance of hydroxyl molecules have previously been found for n-pentane asphaltenes (Moschopedis and Speight 1976b; Ignasiak et al. 1977). However, this peak may actually indicate the presence of water which may be separated together with the asphaltenes because water is more soluble in n-pentane than n-heptane (Yang 2011). Additionally, higher absorbance peaks in the region for other functional groups indicate that n-heptane asphaltenes contain larger proportions of heteroatoms than n-pentane asphaltenes (Speight and Moschopedis 1982).

Another distinctive feature between n-pentane and n-heptane asphaltenes is their aromaticity. As observed from the FTIR spectra, n-heptane asphaltenes appear to have shorter peaks in the aliphatic bond regions (2955-2851 cm^{-1}) but taller peaks in the aromatic bond regions (1600 cm^{-1}) compared to n-pentane asphaltenes (Figure A-1), indicating a higher degree of aromaticity for n-heptane asphaltenes (Speight 1994; Ancheyta et al. 2002). Additionally, when the FTIR spectra of n-pentane and n-heptane asphaltenes are compared to the FTIR spectra of crude oil (Figure A-1), both asphaltenes exhibit higher concentrations of hetero elements, supporting the notion that most of the heteroatoms in the crude oil are concentrated in the asphaltene fraction (Speight 2014). Surprisingly, the peak representing carbonyl functional groups (1700 cm^{-1}) are not clearly distinguishable, more so for the asphaltene samples than the crude oil, due to the noise from atmospheric water vapors (Tennyson et al. 2009).

The FTIR spectra of the asphaltene samples (**Figure A-1**) are also compared with the reference spectra (**Figure A-2**) to ensure that the samples are free of contamination. From this comparison, the samples are not found to show similar peaks with the reference samples. Thus, it can be concluded that the asphaltene samples are free from contamination of solvents and adsorbent materials. However, some anomalies are noticed for sample B2 and W1 (Figure A-1H and A-1K). The FTIR spectrum for the n-pentane asphaltene of B2 exhibit significant peak in the 3600-3100 cm^{-1} region, indicating the large presence of O-H bonds. With the addition of a distinctive peak in the 800-600 cm^{-1} region, the FTIR profile for sample B2 seems identical to distilled water FTIR spectrum shown in **Fig. A-2C**. Since distilled water was not used in asphaltene separation, it is inferred that this sample contain water, especially in the separated asphaltenes. Moreover, similar to its waxy original crude oil, the FTIR spectrum for W1 asphaltenes displayed significant peaks in the C-H bonds region, confirming the presence of wax in the sample.

Further molecular-scale evaluation of asphaltenes are performed through elemental analysis. Elemental composition of the n-pentane asphaltene samples are shown in **Table 5** below.

Table 5: Elemental analysis of n-pentane asphaltene samples

n-Pentane asphaltenes composition											
Elements	**H1†**	**H2**	**H3**	**H4†**	**EH1**	**EH2**	**B1**	**B2†**	**B3**	**B4**	**W1**
C	78.78	79.01	83.87	79.25	81.77	80.4	80.3	66.38	78.59	78.35	80.46
H	7.42	7.81	8.41	7	7.98	8.21	8.19	7.96	8.36	7.63	11.9
H/C	1.13	1.19	1.20	1.06	1.17	1.23	1.22	1.44	1.28	1.17	1.77
O*	3.61	7.02	-2.62	9.25	-0.07	1.79	6.52	13.66	6.47	3.96	6.34
N	1.12	2.43	1.35	1.28	1.84	1.38	1.43	1.06	1.27	1.28	1.03
S	8.83	3.55	8.66	2.61	8.34	7.84	3.38	10.6	5.09	8.51	0.26
Heteroatoms**	13.8	13.18	7.72	13.75	10.25	11.39	11.51	25.66	13.05	14.02	7.64
Trace elements, ppm											
Al	60.5	14.3	n.d.	n.d.	n.d.	n.d.	n.d.	6.34	n.d.	n.d.	n.d.
B	8.3	13.8	58.8	149	11.2	n.d.	6.4	100	7.16	8.71	n.d.
Ca	535	70	27.7	195	n.d.	n.d.	35.6	270	7.96	805	n.d.
Cu	40.1	n.d.	n.d.	n.d.	n.d.	n.d.	n.d.	n.d.	n.d.	n.d.	n.d.
Fe	154	427	107	1340	12.8	761	46.1	46.4	15.5	12	n.d.
K	141	24	53.8	6.53	28	n.d.	26	60	25	91.6	26
Mg	332	18.3	n.d.	13.2	n.d.	n.d.	23.8	22.1	n.d.	57.9	n.d.
Mo	n.d.	13.7	52.7	n.d.	54.9	1460	n.d.	38.1	5.51	29.7	n.d.
Na	764	325	1690	2450	147	34.1	1100	1750	262	65	43.8
Ni	59.5	293	279	201	309	251	172	277	346	260	44.3
P	17	9.6	10	12	9.9	n.d.	11	11	10	11	11
Pb	n.d.	8.37	n.d.	n.d.	n.d.	n.d.	n.d.	n.d.	n.d.	n.d.	n.d.
Si	157	66.6	301	913	n.d.	16.2	n.d.	41	11	6.4	n.d.
Sn	n.d.	17	n.d.	24.1	6	n.d.	n.d.	12	n.d.	n.d.	n.d.
Ti	n.d.	22.1	13.8	n.d.	17.1	n.d.	n.d.	14.3	11.1	n.d.	n.d.
V	145	489	753	793	792	1290	358	775	1490	1310	n.d.
Zn	16.9	5.15	n.d.	9.1	n.d.	n.d.	n.d.	9.01	5.15	n.d.	n.d.
Metals***	2248	1727	2977	5032	1367	3796	1762	3280	2168	2631	114

*O is calculated from the remaining wt%

**Heteroatoms is the sum of every elements (in wt%) except for C and H

***Metals (in ppm) is the sum of all metallic elements (i.e. Al, Ca, Cr, Cu, Fe, K, Mg, Mo, Na, Ni, Pb, Sn, Ti, V, and Zn)

†Samples contain water.

Comparing these data (Table 5) with elemental constituents of crude oil (Table 2), it is clear that asphaltenes are more concentrated with heteroatoms and have higher degree of aromaticity compared to crude oil, which is in agreement with the FTIR spectra. The

effect of these elements on the density of asphaltenes are also analyzed though correlation plots given in **Figure 10**.

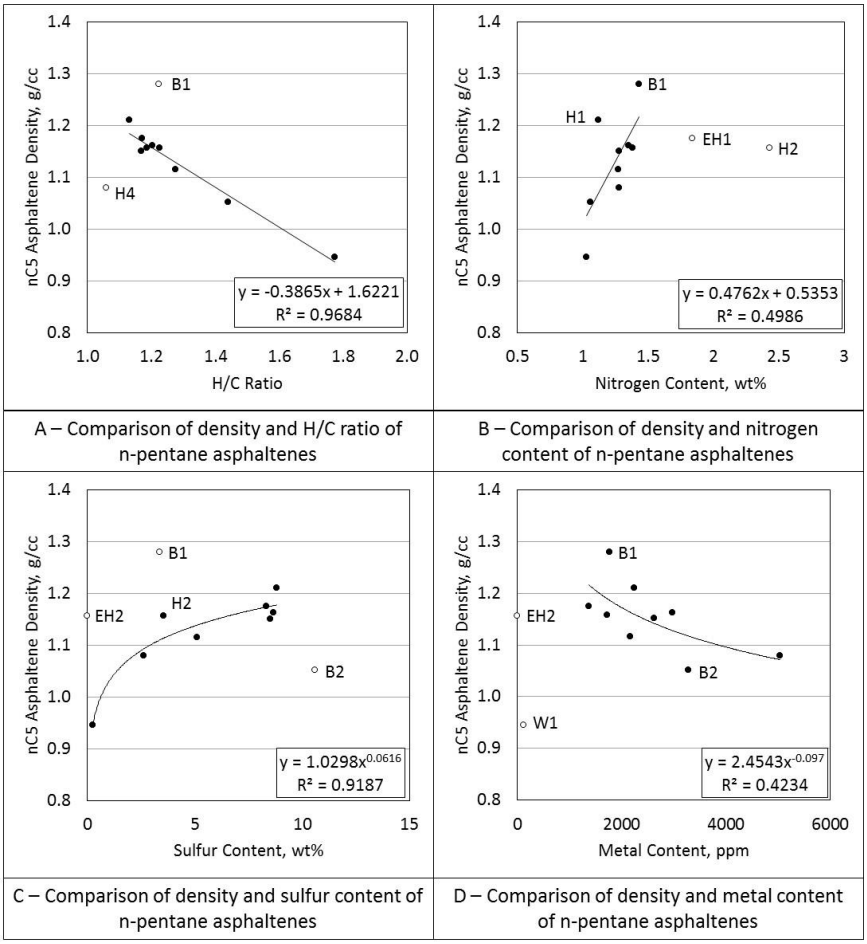

Figure 10: Correlations of elemental composition with density of n-pentane asphaltenes. Blank circles represent outliers in the dataset. Asphaltene densities are reported in Table 4 and elemental analysis data are obtained from Table 5. In Figure 8D, metals include: Al, Ca, Cr, Cu, Fe, K, Mg, Mo, Na, Ni, Pb, Sn, Ti, V, and Zn elements.

Larger proportions of polyaromatic condensed rings, described by the low H/C ratio, is found to contribute to the higher density of asphaltenes, which is in accordance with the literature (Rogel and Carbognani 2003). The increasing amount of sulfur and

nitrogen elements resulted in heavier asphaltenes. On the other hand, oxygen and metal content in asphaltenes are observed to reduce asphaltene density, which is rather counterintuitive. Conceivably, this unique behavior may elucidate the fact that the sulfur and nitrogen compounds have more of a dominant effect on the density of asphaltenes rather than oxygen and other metallic constituents.

This thesis analyzed, for the first time, asphaltene behavior using the zeta potential concept. Zeta potential measurements coupled with particle size analysis on both n-pentane and n-heptane asphaltenes were conducted to evaluate the reliability of these measurements on the estimation of asphaltene stability within the crude oil. The results from these experiments are listed in **Table 6**.

Table 6: Zeta potential and cluster size measurements of asphaltene samples. pH and Total Dissolved Solids (TDS) of the solution are also recorded.

Sample	n-pentane asphaltene				n-heptane asphaltene			
	Cluster Size (nm)	Abs. Zeta Potential (mV)	pH	TDS (ppm)	Cluster Size (nm)	Abs. Zeta Potential (mV)	pH	TDS (ppm)
H1†	905.6	33.95	6.72	198	6943.2	17.40	6.72	198
H2	2337.6	37.03	6.96	88	7093.7	31.66	7.22	176
H3	1888.4	27.63	6.54	86	4114.4	18.20	7.49	167
H4†	3804.4	22.47	7.50	104	891.1	21.48	6.33	78.8
EH1	573.9	34.48	6.27	185	3891.5	23.18	6.27	185
EH2	5796.9	27.09	7.27	102	15224.7	14.41	5.92	102
B1	1739.7	30.86	6.70	172	802.7	17.34	6.70	172
B2†	4766.6	41.60	8.01	93	8877.6	41.80	7.75	173
B3	6279.7	27.42	7.23	173	1757	22.07	7.76	166
B4	1776.6	29.08	6.80	164	6364.9	18.64	7.40	170
W1	1636.5	31.05	6.84	180	267.8	25.26	6.97	170

*The zeta potential and particle size values were obtained from asphaltenes suspended in 1mM KCl solution.
†Samples contain water.

The literature has defined higher absolute values of zeta potential to represent a stable solution while the opposite holds true for lower absolute values (Riddick 1968). Comparing the zeta potential of n-pentane and n-heptane asphaltenes, lower values of zeta potential are observed for n-heptane asphaltenes in almost all of the samples, which implies higher tendency to aggregate, leading to higher polarity and lower stability. This trend agrees with the literature which have consistently found n-heptane asphaltenes to be more polar than n-pentane asphaltenes (Ortega et al. 2015). Only B2 does not follow this trend and has an increase in zeta potential value of 0.2, which may be due to water content of B2. The cluster size of the asphaltenes is also found to be inversely related to the zeta potential values of the asphaltenes. However, H2 and B2 seem to show irregular behavior with the large cluster size that they have despite their high zeta potential value. These inconsistencies may be due to the overestimation of zeta potential that is caused either by the contamination of resin, high pH value of the solution (Parra-Barraza et al. 2003; Hannisdal et al. 2006), or water content of bulk oil which cannot be separated through n-pentane treatment (Yang 2011).

When composition of SARA fractions (Table 1) is taken into consideration in **Figure 11**, asphaltene content exhibit linear relationship with cluster size of the samples. This trend may suggest that higher concentration of asphaltenes increase the chances of asphaltenes molecules to come into contact with each other, leading to more aggregation and increase in cluster size. Resins and aromatics weight percent also correlate linearly with zeta potential, emphasizing their roles in stabilizing asphaltenes within the crude oil. Zeta potential is also shown to increase as the ratio of resins-to-asphaltenes increases,

further signifying the peptizing ability of resins (Jada and Salou 2002). These results have proven that interaction between the polar compounds of crude oil are important to be analyzed because they can affect the overall polarity of the sample (Kar and Hascakir 2015).

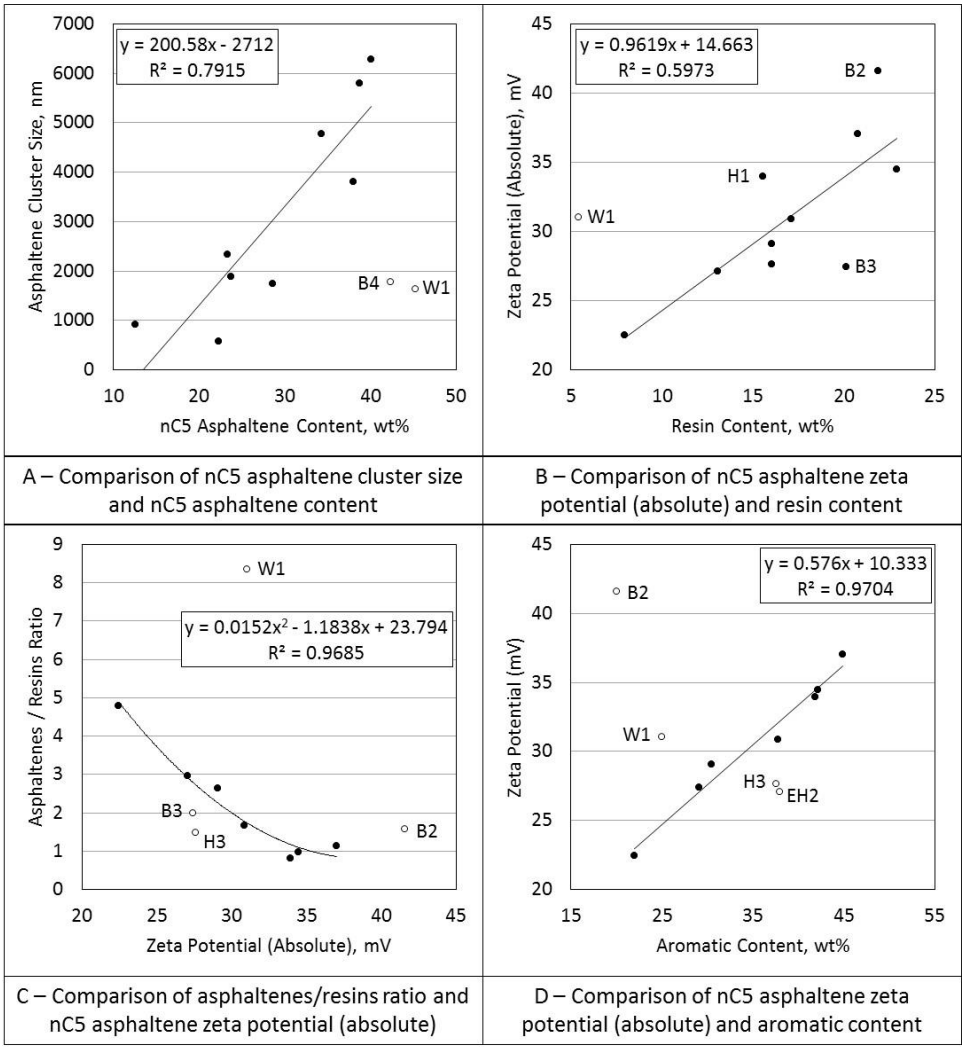

Figure 11: Correlations of SARA fractions (Table 1) with zeta potential and cluster size of n-pentane asphaltenes (Table 6). Blank circles represent outliers in the dataset.

The zeta potential and cluster size values are also correlated with elemental composition of n-pentane asphaltenes to determine the functional group that is responsible for stability of asphaltenes. From the correlation plots in **Figure 12**, higher degree of condensation for the polycyclic aromatic hydrocarbons (PAH) signified by the low H/C ratio is found to create more stable asphaltene molecules (Ruiz-Morales 2002; Ruiz-Morales and Mullins 2007). Some anomalies can still be observed, however, which may be due to the contribution of some inorganic carbon compounds that can deviate the H/C ratio. The presence of oxygen and, to a lesser extent, nitrogen cause asphaltenes to become more polar as implied by the decrease in zeta potential of the asphaltenes. However, an inconsistency is observed for the sulfur element, where increasing concentration of sulfur leads to higher stability of asphaltenes. This trend seems implausible because the existence of heteroatoms within the asphaltene molecule causes charge imbalances on the atomic scale and should generate permanent electrical dipoles, making the molecule more polar (Wattana et al. 2005). In contrast, the metallic components contribute to higher polarity of the asphaltene molecules as expected (Kaminski et al. 2000; Nalwaya et al. 1999).

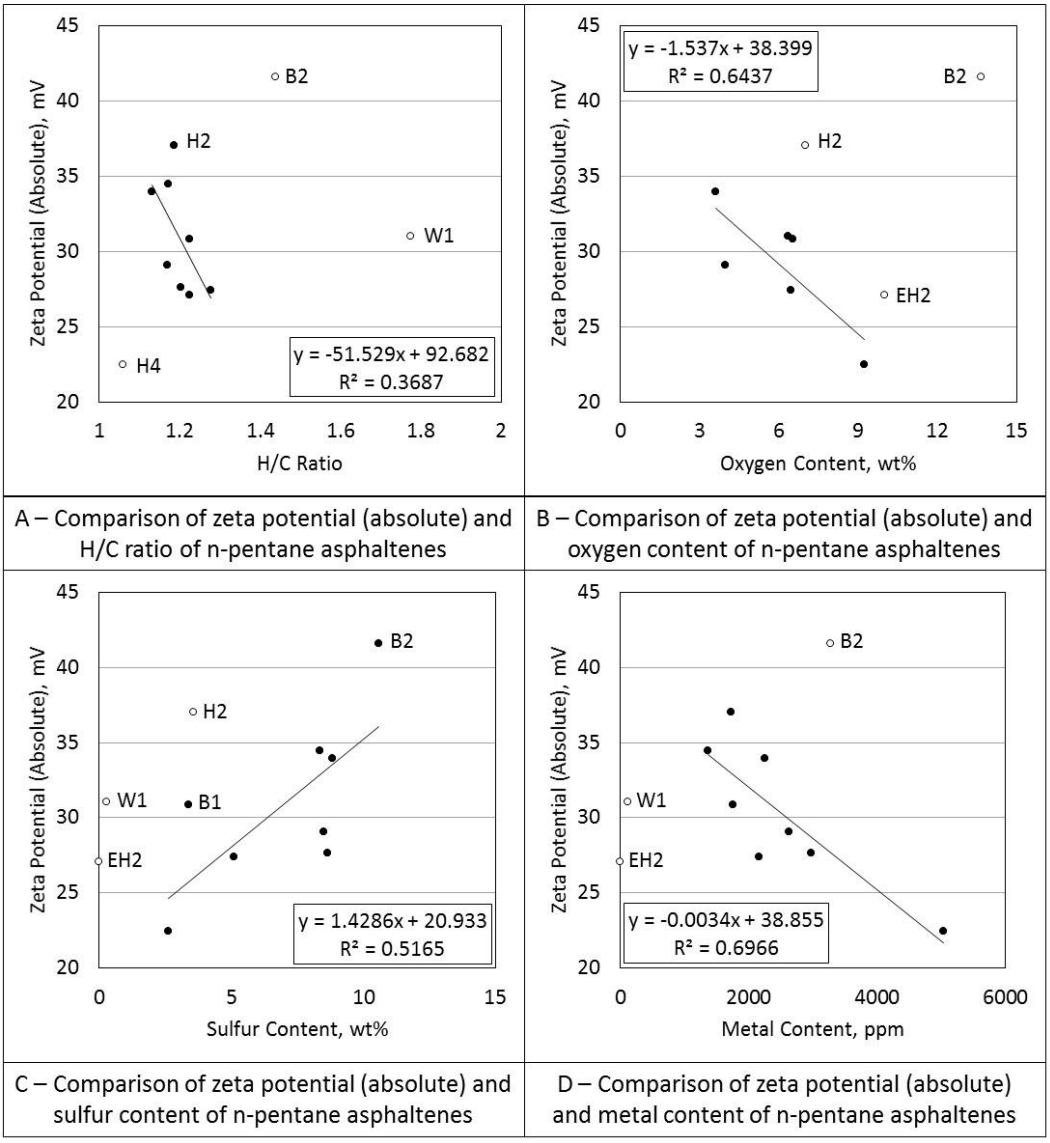

Figure 12: Correlations of elemental composition of nC_5 asphaltenes (Table 5) with zeta potential of nC_5 asphaltenes (Table 6). Blank circles represent outliers in the dataset. Metal content is the summation of all metallic elements, which include Al, Ca, Cr, Cu, Fe, K, Mg, Mo, Na, Ni, Pb, Sn, Ti, V, and Zn.

When the elemental composition of the n-pentane asphaltenes are compared with the cluster sizes in **Figure 13**, some of the functional groups are proven to have clear-cut influence on asphaltene polarity. Oxygen moieties are revealed to increase the tendencies of asphaltene molecules to aggregate in larger clusters, which is in accordance to the

previous zeta potential results (based on Table 5 and 6). Similarly, the metal contents are also enhancing the polarity of asphaltene molecules as indicated by the increase in cluster size (Figure 13). In contrast, the sulfur and nitrogen functional groups are exhibiting inconsistent trends when correlated with asphaltene cluster sizes (Table 5 and 6).

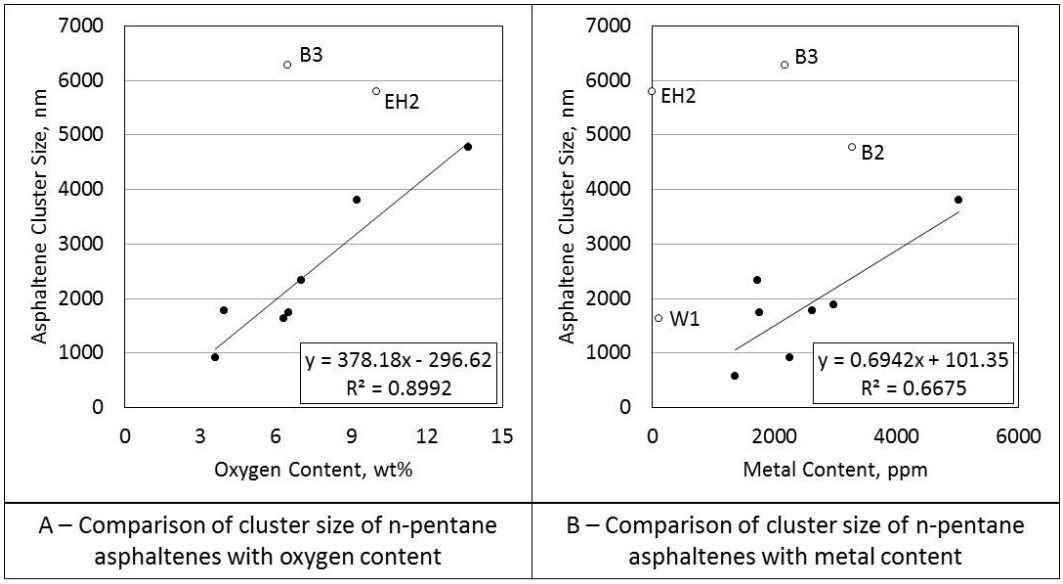

Figure 13: Correlations of elemental composition of nC_5 asphaltenes (Table 5) with cluster size of nC_5 asphaltenes (Table 6). Blank circles represent outliers in the dataset.

Asphaltene stability was investigated through several microscopy technique to observe the aggregation behavior of asphaltenes that have been precipitated under different conditions. Visual inspection from optical microscopy in **Figure 13** shows how some asphaltenes tend aggregate in smaller clusters while others form larger clusters. Asphaltenes precipitated from n-heptane are exhibiting larger clusters compared to the n-pentane asphaltenes, corroborating the high polarity nature of n-heptane asphaltenes. It should be noted that the asphaltenes clusters can easily break during sample preparation

or microscopic observation. Also, asphaltenes are highly oxidative, hence, these images should be acquired just after asphaltene separation and measurements should be conducted quickly. However, if separation and imaging can be accomplished under inert atmosphere, interpretation of images would be more useful to understand asphaltene stability.

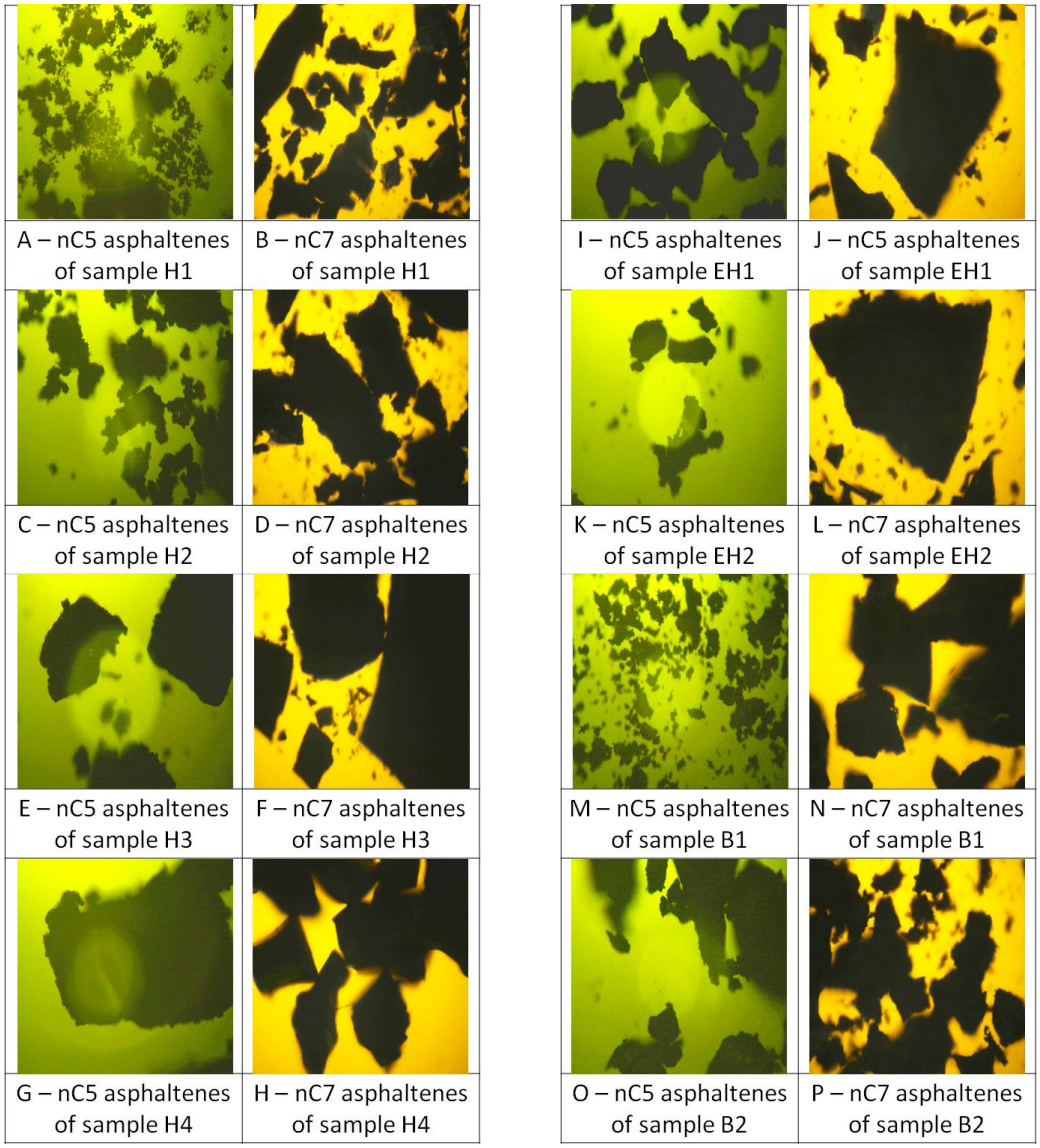

Figure 14: Optical microscopic images for nC_5 and nC_7 asphaltenes under 100X magnification

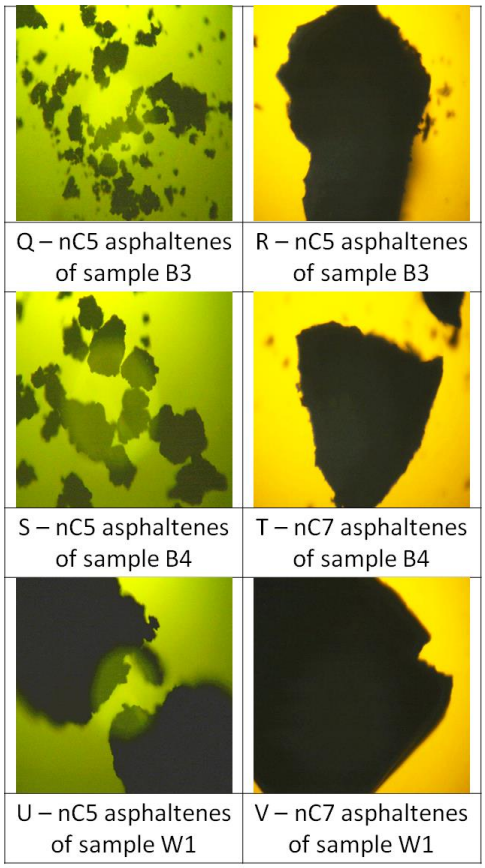

Figure 14: Continued

To investigate the surface chemistry and morphology of asphaltenes, SEM-EDS imaging was also conducted. **Figure 15** are examples of SEM images and **Table 7** lists the EDS results of n-pentane asphaltenes. As seen in Figure A-6, asphaltenes from different origins show a wide variety of surface morphology, from really smooth surfaces to clustered and rough surfaces.

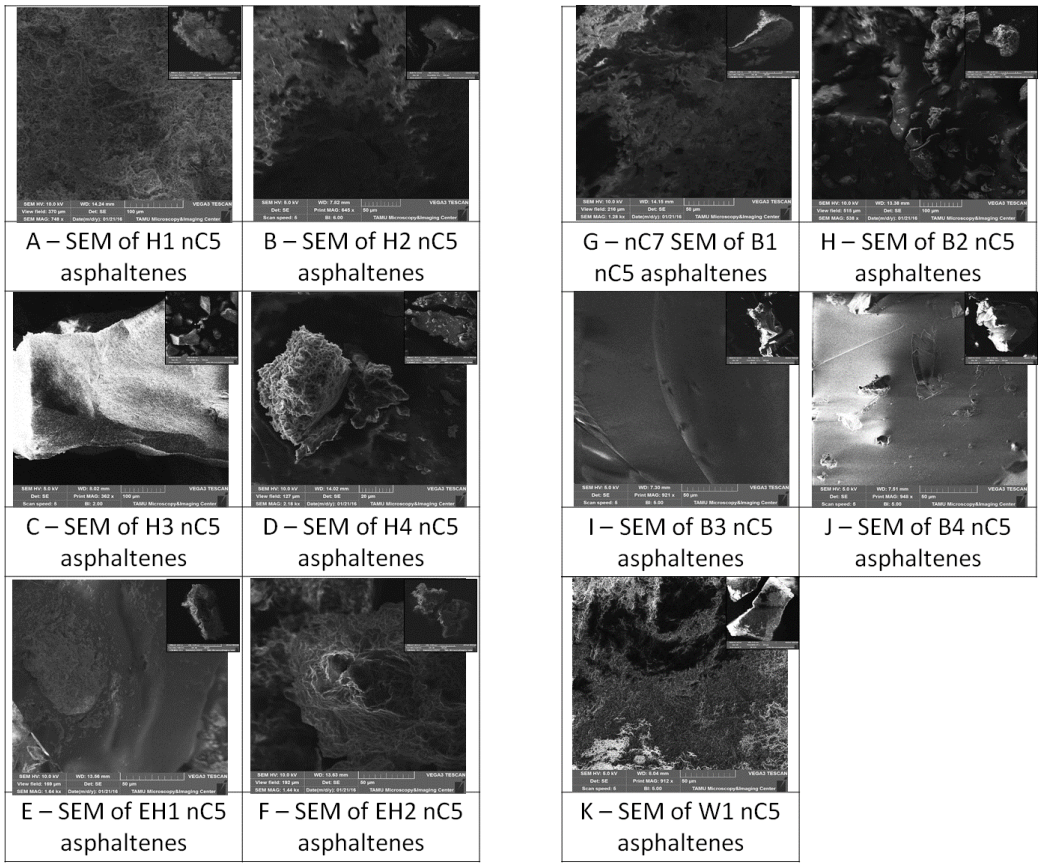

Figure 15: SEM images of n-pentane asphaltenes

Interestingly, almost all of the EDS (Table 7) did not detect the presence of the nitrogen and heavy metals, even though they are the primary constituents of asphaltenes and are known to be present within the samples based on the elemental analysis results (Table 5). Other than for sample H1, sulfur wt% in the other samples are also significantly smaller than expected. Since EDS only have depth resolution of around 1-5 μm (Lee 2002; Klein and Hercules 1983), the EDS may not be able to capture elements transmitted from the core of asphaltenes, implying that the heavier elements are contained within the core of asphaltenes rather than on the exterior ends (Speight 2014). In contrast, oxygen is abundantly found on the surfaces of asphaltenes due to the oxidative nature of asphaltenes

(Moschopedis and Speight 1975). Furthermore, the EDS results show the presence of chlorine (Cl) which was not detected previously in the elemental analysis of asphaltenes (Table 5). The source of Na and Cl elements may be from contamination of crude oil by the reservoir brines (Tang and Morrow 1999).

Table 7: EDS results of n-pentane asphaltenes

n-Pentane asphaltenes surface elements											
Elements, wt%	**H1†**	**H2**	**H3**	**H4†**	**EH1**	**EH2**	**B1**	**B2†**	**B3**	**B4**	**W1**
C	89	87.73	91.1	80.9	87.9	93.1	88.8	89.2	88.02	89.87	91.67
O	2	10.87	7.9	18.7	10.8	4.4	8.6	6.6	10.13	8.47	8.1
S	8.6	0.87	0.6	0.2	0.6	2.2	2.3	2.8	0.59	1.29	0.02
N	0	0	0	0	0	0	0	0.8	0	0	0
Al	0.2	0.16	0.3	0.1	0.5	0.2	0.1	0.1	1.11	0.21	0.19
Ca	0.1	0	0	0	0	0	0	0	0	0	0
Cl	0	0.07	0	0	0	0	0	0.1	0.04	0.08	0
Cr	0	0	0	0	0	0	0	0	0	0	0
Fe	0	0.03	0	0	0	0	0	0	0	0	0
Mg	0	0.01	0	0	0	0	0	0	0.07	0.01	0.01
Na	0	0.21	0.1	0	0	0	0	0.2	0	0.07	0
Ni	0	0	0	0	0	0	0	0	0.03	0	0
Si	0	0.05	0	0	0	0	0	0	0.01	0.01	0.01
V	0	0.01	0	0	0	0	0	0	0	0	0

*EDS cannot detect hydrogen.
†Samples contain water.

To understand the role of surface elements in the aggregation mechanism of asphaltene molecules, the EDS results (Table 7) were correlated with zeta potential and cluster size of asphaltenes (Table 6) in **Figure 16**.

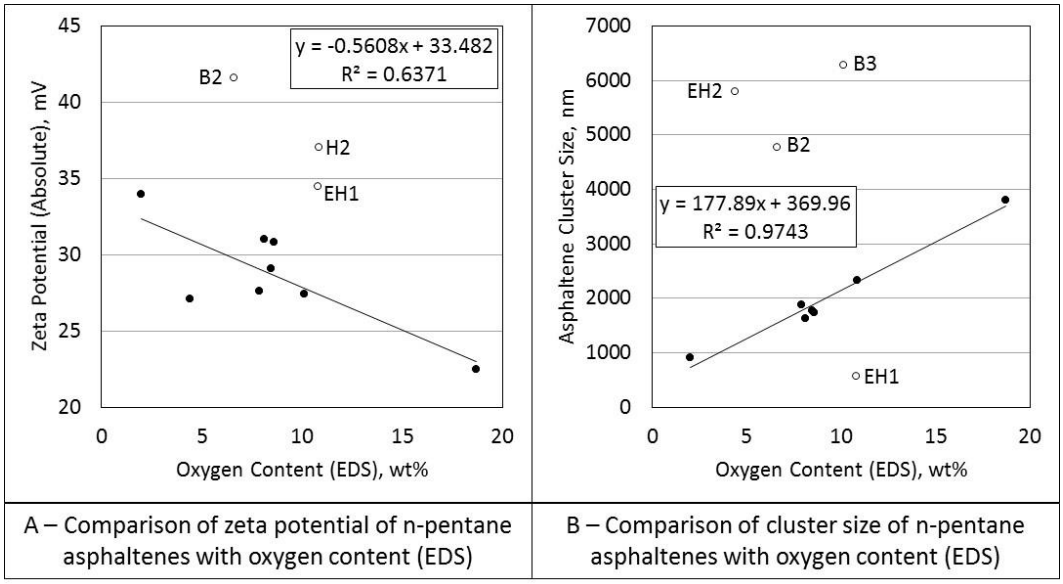

A – Comparison of zeta potential of n-pentane asphaltenes with oxygen content (EDS)

B – Comparison of cluster size of n-pentane asphaltenes with oxygen content (EDS)

Figure 16: Correlation of oxygen content (EDS) with zeta potential and cluster size of n-pentane asphaltenes. Blank circles represent outliers in the dataset.

The abundance of oxygen functions in the form of hydroxyl groups at peripheral sites of asphaltene molecules have previously been observed (Moschopedis and Speight 1976b) and their effects on asphaltene stability analyzed (Moschopedis and Speight 1976a). Comparison of zeta potential and cluster size data with oxygen content from the surface of asphaltenes (Figure 16) shows that oxygen moieties, most likely to be in hydroxyl structure, can cause asphaltene molecules to have higher propensity towards aggregation. This result falls in agreement with the literature which signifies the importance of hydrogen bonds in asphaltene agglomeration mechanism (Moschopedis and Speight 1976a). Note that oxygen could be added to asphaltene due to exposure to air. Nevertheless, this information is crucial to understand the oxidation tendencies of asphaltenes, which can have a direct impact on asphaltene stability.

Another attempt to characterize the cluster size of asphaltenes when suspended in toluene is through the use of AFM microscopy. **Figure A-4** presents the 3D image of the particles that are contained within the toluene solution. However, obtaining a representative result from this experiment proved to be difficult due to the really small scale of observation. Accurate measurements were also hard to perform because of the impurities contained within the toluene solvent, even though an ACS reagent grade (≥99.5%) have been used to dilute the samples. Through comparison of the images in Figure A-5, it is evident that the impurities within the toluene solvent can also exhibit peaks, creating noises that are hard to differentiate with signs of the asphaltene particles. When just the sample holder (mica) was analyzed, no peaks can be seen, which means that the noise should only come from the impurities in toluene. Hence, to achieve accurate measurements with AFM microscopy, the toluene solvent used to dilute the asphaltenes should have 100% purity, which is quite hard and costly to attain.

4.3 Onset Asphaltene Precipitation Results

Different volumes of n-pentane or n-heptane were mixed with the bulk samples to precipitate asphaltenes. The results from these tests are given in **Table 8**. Comparison of the outcome from n-pentane and n-heptane showed that higher carbon number of n-alkane precipitate lower amount of asphaltenes (Buenrostro-Gonzalez et al. 2004). Some discrepancies are found for sample EH2 and B2 where increasing concentration of solvent ratio actually decreases the amount of precipitated asphaltenes, though, this trend have also been observed previously in heavy oil samples (Kokal et al. 1992). For most of the

viscous samples, the low solvent ratios produce inaccurate results. These error may be caused by experimental challenges related to filtration of highly viscous samples or the erroneous nature of asphaltene precipitation at low solvent ratios (Speight et al. 1984). The insufficient proportions of solvents to completely separate resin from asphaltenes at lower solvent ratios may be another explanation for these high amount of precipitation (Speight 1994; Speight et al. 1984).

Table 8: Onset asphaltene precipitation results for n-pentane and n-heptane

Solvent Ratio*	H1		H2		H3		H4		EH1		EH2	
	nC_5	nC_7	nC_5	nC_7	nC_5	nC_7	nC_5	nC_7	nC_5	nC_7	nC_5	nC_7
1	6.64	0.77	26.57	5.80	7.26	3.14	26.86	8.42	15.66	2.51	23.66	16.33
3	8.82	1.24	35.77	7.78	9.57	3.44	29.50	7.51	16.68	11.13	26.83	23.69
5	6.93	1.07	23.87	10.75	14.90	4.07	31.72	9.34	17.66	11.77	27.79	22.50
10	12.14	1.72	23.35	11.15	14.00	5.71	33.75	8.26	20.70	13.40	29.91	21.42
30	13.33	6.80	28.30	12.73	13.80	7.64	32.69	12.92	26.94	15.94	23.94	18.55

Solvent Ratio*	B1		B2		B3		B4		W1	
	nC_5	nC_7	nC_5	nC_7	nC_5	nC_7	nC_5	nC_7	nC_5	nC_7
1	15.41	9.27	34.61	5.63	47.02	33.65	67.71	55.97	37.81	28.61
3	12.78	9.85	32.34	25.92	47.86	23.41	57.52	45.80	39.48	28.07
5	19.40	10.40	38.98	30.21	35.09	16.29	42.62	37.24	39.71	14.68
10	16.13	9.90	42.76	30.41	40.08	21.27	42.41	37.74	45.30	24.01
30	22.51	9.43	32.46	27.52	36.64	20.81	53.89	40.63	45.51	24.85

*Solvent ratio is mL of solvent / g of oil

Oil composition continuously changes during production due to the variation in pressure and temperature throughout the production system (McCain 1990). To model this operating condition, the saturate fraction is used to alter the chemical composition of the crude oil. Pseudo mixture of saturates fraction and H1 crude oil was prepared and the OAP was repeated. From **Figure 16**, it can be observed that the addition of saturate fraction

induces larger amount of asphaltene precipitation. It can be observed from the graph that the addition of saturate induces larger amount of precipitated asphaltenes as compared to n-pentane and n-heptane asphaltenes, thus, highlighting lower solvating power and stronger destabilization force of the saturate fraction of the crude oil as compared to n-pentane and n-heptane. Therefore, precipitation of asphaltene during production can actually accelerate further precipitation due to increasing volume percentage of saturate fraction in the crude oil, resulting in a more severe asphaltene depositional problem. This characteristic is opposite that of resins and aromatics which are found to stabilize asphaltene in solution (Parra-Barraza et al. 2003).

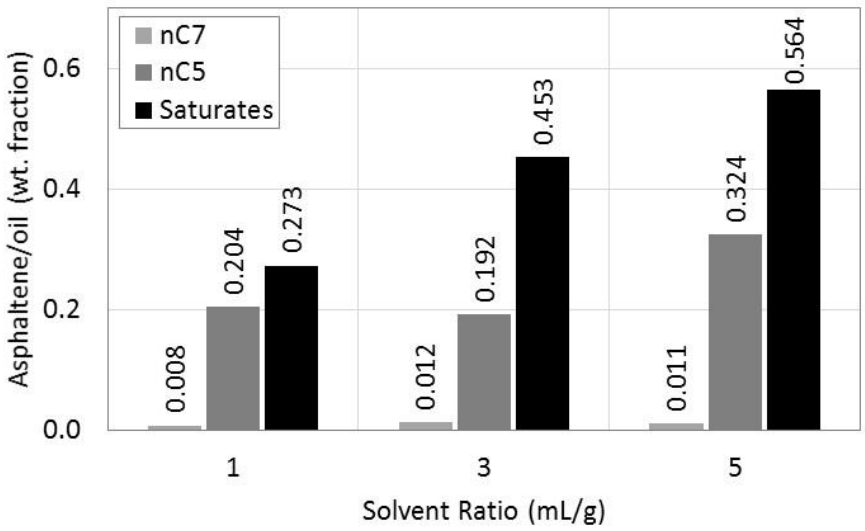

Figure 17: Onset asphaltene precipitation tests with saturate fraction and n-pentane for sample H1

In accordance to the OAP results, because saturates fraction precipitated more asphaltenes, the carbon number of the straight chain aliphatic saturates fraction of the

crude oil was expected to be lower than 5. However, the absorbance peaks which indicate the aliphatic regions in FTIR spectra give the lowest magnitude for nC5, intermediate for nC7, and the highest for saturates fraction of H1 (**Figure 18**). This contradiction highlights that in addition to the straight chain structure, saturates originated from bulk crude oils may also have branched but saturated structure and may contain functional groups, or heteroatoms. Presence of impurities in the saturate fraction of the crude oil has been previously reported by He et al. (2013). There are a few studies on how the asphaltene destabilization is established by the addition of saturated hydrocarbons with cyclic structures, or branched chained saturated hydrocarbons with impurities (Mukhametshina et al. 2015; Pereira et al. 2011; Wiehe et al. 2005).

Also, the analysis of the FTIR spectra of saturates fractions may further elaborate the behavior of asphaltenes when the saturates fraction of crude oil increases. The FTIR spectra of the saturates fraction of sample H1 shown in Figure 18**,** indicates high absorbance peaks corresponding to hydrocarbon bonds of n-alkane. In addition to the normal alkane absorbance signature, the wavenumber region specified by the red arrow at the peak around 950-910 cm^{-1} may correspond to the presence of functional groups with impurities (Silverstein and Bassler 1967). The polarity associated with the functional groups and heteroatoms can significantly alter the overall polarity of the saturate fraction and consequently cause more asphaltene precipitation (Clayden 2001; Reichardt 1988; Skoog et al. 2014; Rappoport 2003).

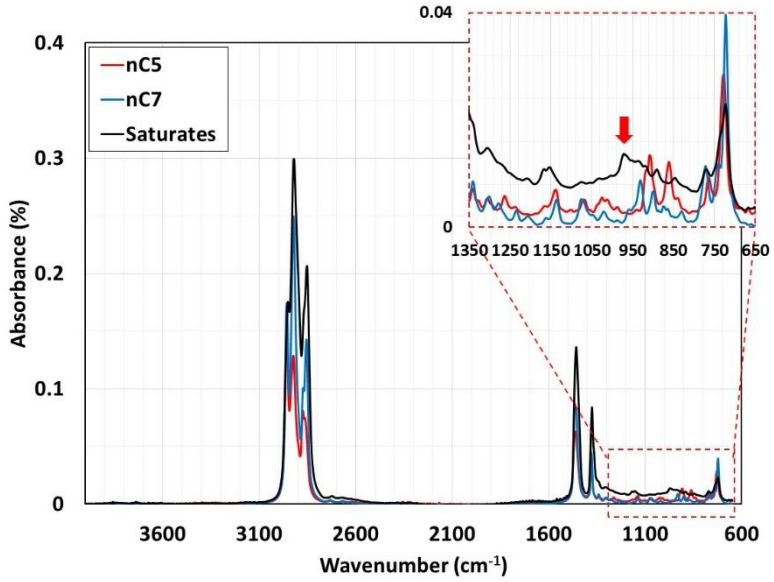

Figure 18: FTIR spectra of n-pentane, n-heptane, and saturate fraction of H1.

The FTIR spectra of all saturates fractions originated from 11 crude oil samples were examined and are included in the appendix section (**Fig. A-5**). Possible signature of similar functional groups were observed in all the saturates fractions, with H1 saturate sample yielding the highest absorbance peak in the signature region. Interpretations of these signatures in FTIR spectra are difficult, however, these peaks are the indication of presence of impurities in saturates fractions.

Additional experiments were conducted to validate the presence of impurities within the saturates fraction and identify its molecular functionalities. First of all, Thermogravimetric Analysis and Differential Scanning Calorimetry (TGA-DSC) were conducted on the saturates fraction of sample H1 and B2 as well as n-heptane and n-decane for comparison purposes. TGA-DSC analyses were carried out under air injection by applying 10 °C/min heating rate and the temperature was increased till 900 °C. From the TGA-DSC curve in **Figure 19**, it can be observed that at 62 °C and 150 °C, respectively,

n-heptane and n-decane are completely consumed (purple and green TGA curves, respectively). At the same temperature values, DSC curves indicate endotherms (peaks) which are the indication of evaporation of these solvents. After those chemicals are consumed, DSC curve does not indicate any endothermic or exothermic reactions. However, saturates fractions are consumed at around 400 °C (black and red TGA curves). At the same temperature, DSC curves show a deep valley which is the indication of exothermic reactions. DSC curve between 320 – 500 °C shows several exotherms (valleys) and endotherms (peaks) which indicates the presence of impurities in saturates fraction.

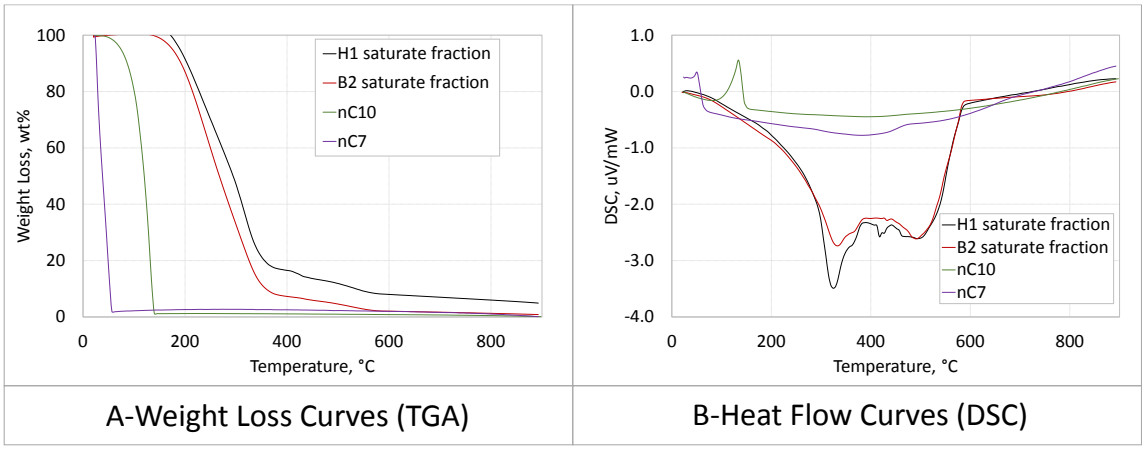

Figure 19: TGA and DSC curves for nC7 (purple curves), nC10 (green curves), and saturate fractions of sample H1 (black curves) and B2 (red curves).

After confirming the presence of impurities with FTIR and TGA-DSC analyses, we also conducted Nuclear Magnetic Resonance (NMR) spectroscopy to further understand the molecular structure of the saturates fraction. From **Figure 20**, the proton NMR spectrum revealed that there is a possibility of carboxylic acids (O-H bond) as shown by the small peak. In contrast, no carbonyl peaks are observed from the 13C NMR

spectrum, this can be due to the lower sensitivity of 13C spectra (S/N ratio of 913:1) compared to 1H spectra (S/N ratio of 4300:1). Still the sensitivity of these measurements methods highly depends on the amount of the component (oxygen or sulfur) present in the sample. In other words, if the impurity content is below the detection limit of NMR, then, the impurity may not appear in the spectrum.

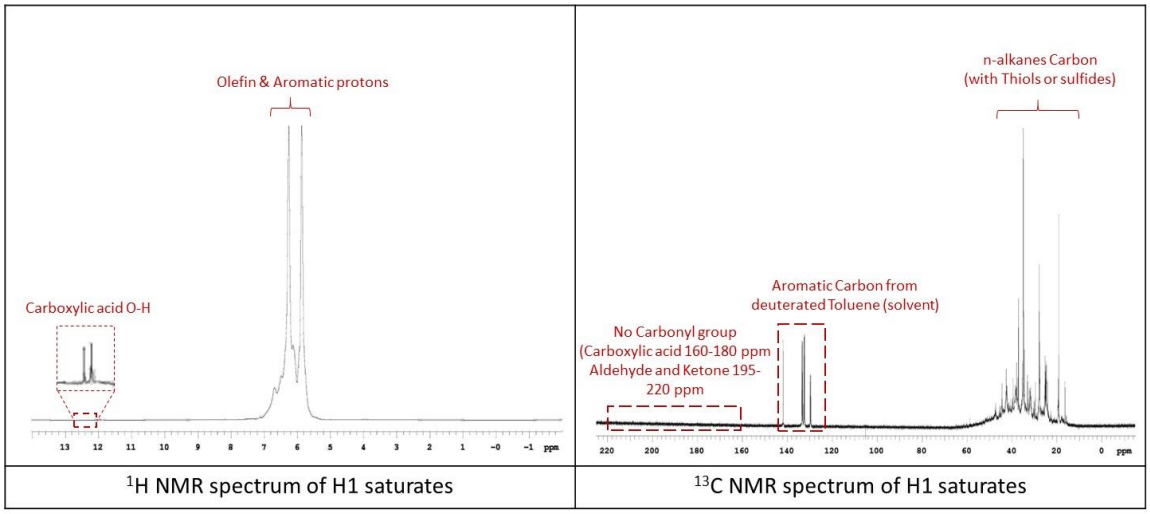

Figure 20: 1H and 13C NMR spectroscopy of saturate fraction of sample H1.

The Electrospray Ionization-Mass Spectrometry (ESI-MS) analysis was also conducted on the saturates sample of H1. Comparison of the resulting spectrum with available spectrums in online databases (http://www.massbank.jp/SearchPage.html) lead to many matches with compounds containing oxygen compounds and also provide some matches with compounds containing sulfur and phosphates functional groups. The positive and negative ions ESI-MS are given in **Figure 20 and 21**.

While the existing libraries are rich, since the saturates fraction is a complex hydrocarbon mixture, no exact match for the saturates fraction was found in the library.

However, while these results could not provide us the presence of sulfur groups, it still proves the existence of impurities in saturates fraction.

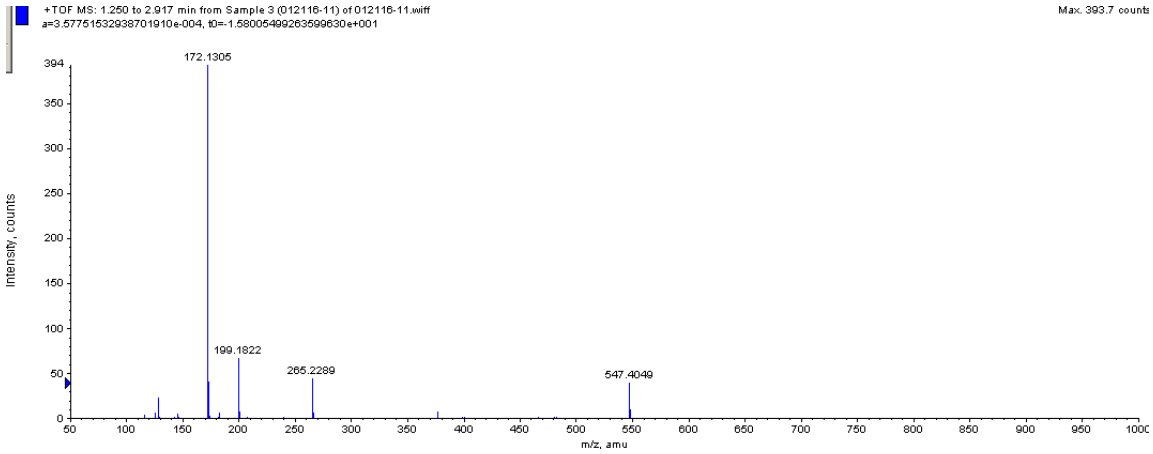

Figure 21: Positive ions ESI-MS of H1 saturate fraction

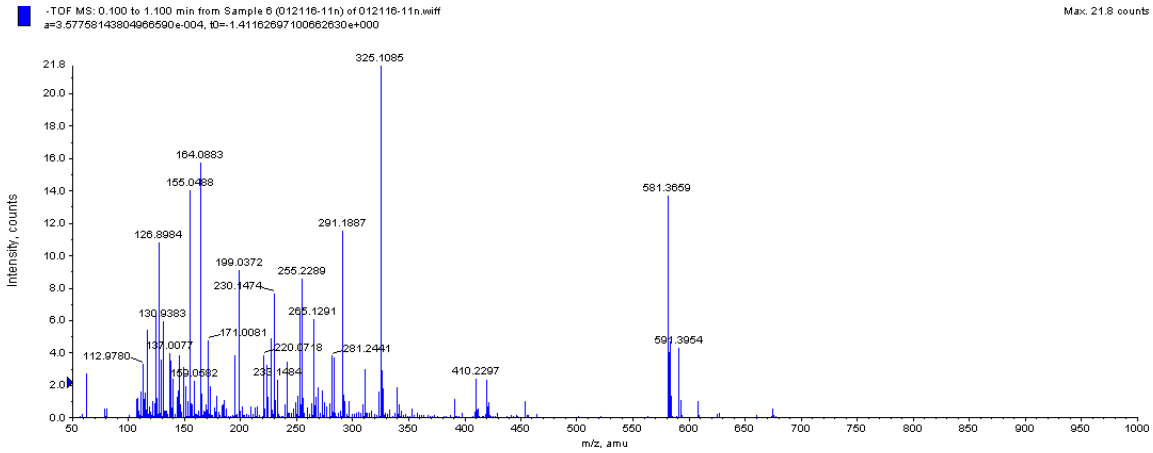

Figure 22: Negative ions ESI-MS of H1 saturate fraction

Finally, SEM-EDS analysis was also conducted on the saturates fraction of sample H1 and B2 to analyze their elemental compositions. To analyze these liquid samples, the saturates samples were dropped onto two (an organic and an inorganic) filter papers and dried under the vacuum oven. The dried filter papers were then analyzed under SEM-EDS

microscope. The initial filter paper was also analyzed through SEM-EDS for comparison purposes. EDS results and SEM images of the samples are given **Table 9** and **Figure 23**.

Table 9: EDS results of nylon (organic) and silver (inorganic) membranes and saturate fractions of sample H1 and B2.

Elements	0.45 µm Nylon Membrane			0.20 µm Silver Membrane		
	Membrane Only	H1	B2	Membrane Only	H1	B2
C	73.67	85.83	87.40	16.45	73.78	75.78
O	19.90	14.13	12.43	0.00	1.49	1.42
N	6.43	0.00	0.00	0.00	0.00	0.00
S	0.00	0.40	0.17	0.00	0.00	0.00
Mg	0.00	0.00	0.00	1.32	0.37	0.30
Ag	0.00	0.00	0.00	82.22	24.37	22.49

The EDS results confirm the presence of oxygen within the saturates fraction for both H1 and B2 for the measurements conducted both with nylon and silver membranes. However, nylon membrane also shows the presence of sulfur in very low quantity. Even though, both membranes have high resistance to several chemicals, with this study, these membranes have been tested for the first time with saturates.

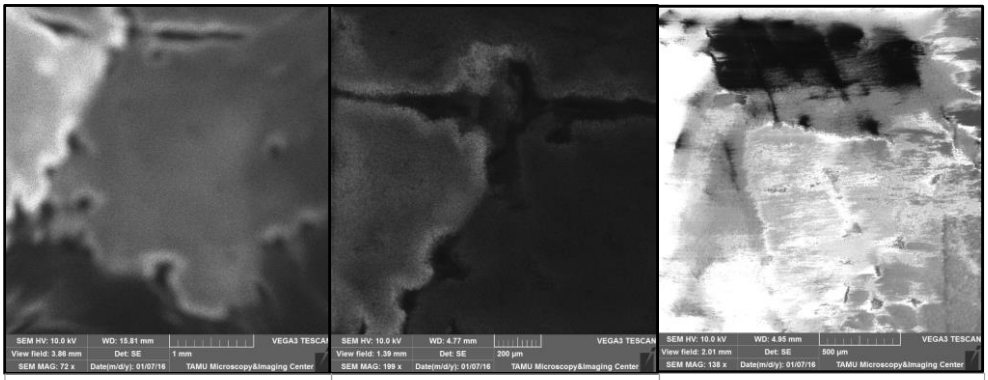

A- SEM of Nylon Membrane

B- SEM of H1 Saturates on Nylon Membrane

C- SEM of B2 Saturates on Nylon Membrane

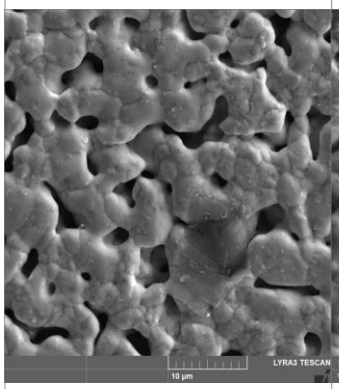

D- SEM of Silver Membrane

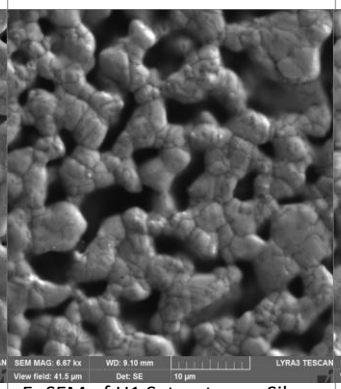

E- SEM of H1 Saturates on Silver Membrane

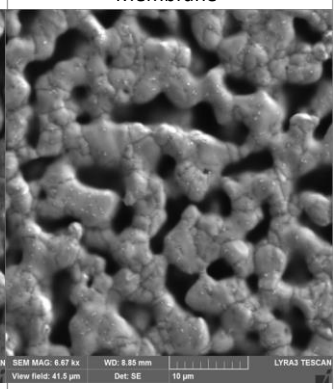

F- SEM of B2 Saturates on Silver Membrane

Figure 23: SEM Images of A-Nylon Membrane (organic), B- Nylon Membrane with H1 Saturates, C- Nylon Membrane with B2 Saturates, D-Silver Membrane (inorganic), E- Silver Membrane with H1 Saturates, F- Silver Membrane with B2 Saturates.

The SEM images revealed that the pores of the silver membrane after exposure to saturates fraction are larger than the original silver membrane (0.20 microns pore size). This observation may imply that a reaction occurred between the silver membrane and the components of the saturates fraction which causes a damage in the silver membrane. With previous studies signifying the high affinity of carboxylic acids to bond with silver (Schlotter et al. 1986; Wang et al. 1998; Quaroni and Chumanov 1999), this finding indicates a possibility that the saturate fraction may contain carboxylic acid compounds.

However, the possibilities of sulfur functional groups occuring within the saturates fraction still exist. Silver complexation with sulfur organics is also a known phenomenon (Bell and Kramer 1999). However, the damage in membranes and possible low concentration of sulfur in saturates fraction was not sufficient to observe the complexation. Still, it can be concluded that the saturates fractions has oxygen and may also contain sulfur functional groups.

CHAPTER V

CONCLUSIONS

In this thesis, 11 different crude oils and bitumens and their separated n-pentane and n-heptane asphaltenes were analyzed to investigate the variables pertaining to the destabilization mechanism of asphaltenes. Physicochemical correlations were also examined to generate a simple yet universal technique to estimate asphaltene stability.

Characterization of the crude oil have signified that heavier and more polar components of the crude oil, i.e. asphaltenes and resins, have a predominant role in shaping up the physicochemical characteristics of crude oil. Heteroatoms such as nitrogen, oxygen, sulfur, and metallic elements are revealed to contribute to higher levels density, viscosity, and asphaltene content of the crude oil.

The presence of polar functionalities within the asphaltene molecules have been proven to increase the overall polarity of asphaltenes. Oxygen and metallic functional groups, in particular, have shown great correlations with zeta potential and cluster size of asphaltenes. Microscopic images also revealed n-heptane asphaltenes form bigger clusters than n-pentane which might be the indication of higher polarity of n-heptane asphaltenes than n-pentane asphaltenes. Comparison of SEM-EDS with elemental analysis results also verified the location of heteroatoms to be at the core of the asphaltene molecules, except for hydroxyl functional groups.

Finally, onset asphaltene precipitation results have reaffirmed the destabilizing power of the saturate fraction. Thus, the higher concentration of saturate fraction within the crude oil can pose higher risks of asphaltene-related issues.

REFERENCES

Akbarzadeh, K., Alboudwarej, H., Svrcek, W.Y. et al. 2005. A generalized regular solution model for asphaltene precipitation from n-alkane diluted heavy oils and bitumens. *Fluid Phase Equilibria* **232** (1-2): 159-170.

Akbarzadeh, K., Hammami, A., Kharrat, A. et al. 2007. Asphaltenes-Problematic but Rich in Potential. *Oilfield Review*: 22-43.

Akbarzadeh, Kamran, Dhillon, Amandeep, Svrcek, William Y. et al. 2004. Methodology for the Characterization and Modeling of Asphaltene Precipitation from Heavy Oils Diluted with n-Alkanes. *Energy & Fuels* **18** (5): 1434-1441. 10.1021/ef049956b.

Ali, M. A., Livingstone, S. E. 1974. Metal complexes of sulphur-nitrogen chelating agents. *Coordination Chemistry Reviews* **13** (2–3): 101-132. http://dx.doi.org/10.1016/S0010-8545(00)80253-2.

Alkafeef, S.F., Al-Medhadi, F., Al-Shammari, A.D. 2005. A Simplified Method To Predict and Prevent Asphaltene Deposition in Oilwell Tubings: Field Case. *SPE Production & Facilities* **20** (02): 126-132. SPE-84609-PA. http://dx.doi.org/10.2118/84609-PA.

Ancheyta, J., Centeno, G., Trejo, F. et al. 2002. Extraction and Characterization of Asphaltenes from Different Crude Oils and Solvents. *Energy & Fuels* **16** (5): 1121-1127. 10.1021/ef010300h.

ASTM D4124-09. Standard Test Method for Separation of Asphalt into Four Fractions. 2009. West Conshoshocken, PA: ASTM International.

ASTM D2007-11. Standard Test Method for Characteristic Groups in Rubber Extender and Processing Oils and Other Petroleum-Derived Oils by the Clay-Gel Absorption Chromatographic Method. 2011. West Conshohocken, PA: ASTM International.

ASTM D3279-12. Standard Test Method for n-Heptane Insolubles. 2012a. West Conshoshocken, PA: ASTM International.

ASTM D6560-12. Standard Test Method for Determination of Asphaltenes (Heptane Insolubles) in Crude Petroleum and Petroleum Products. 2012b. West Conshoshocken, PA: ASTM International.

ASTM D893−14. Standard Test Method for Insolubles in Used Lubricating Oils. 2014. West Conshoshocken, PA: ASTM International.

Barrera, D.M., Ortiz, D.P., Yarranton, H.W. 2013. Molecular Weight and Density Distributions of Asphaltenes from Crude Oils. *Energy Fuels* **27** (5): 2474-2487.

Barwise, A. J. G. 1990. Role of nickel and vanadium in petroleum classification. *Energy & Fuels* **4** (6): 647-652. 10.1021/ef00024a005.

Bayliss, Peter, Levinson, A.A. 1976. Mineralogical review of the Alberta oil sand deposits (Lower Cretaceous, Mannville Group). *Bulletin of Canadian Petroleum Geology* **24** (2): 211-224.

Bell, Russell A., Kramer, James R. 1999. Structural chemistry and geochemistry of silver-sulfur compounds: Critical review. *Environmental Toxicology and Chemistry* **18** (1): 9-22. 10.1002/etc.5620180103.

Bellamy, L.J. 1980. *The Infrared Spectra of Complex Modules*, Vol. 2. London: Advances in Infrared Group Frequencies, Springer.

Benkhedda, Zouhir, Landais, Patrick, Kister, Jacky et al. 1992. Spectroscopic analyses of aromatic hydrocarbons extracted from naturally and artificially matured coals. *Energy & Fuels* **6** (2): 166-172. 10.1021/ef00032a008.

Bennett, P. C., Siegel, D. E., Baedecker, M. J. et al. 1993. Crude oil in a shallow sand and gravel aquifer—I. Hydrogeology and inorganic geochemistry. *Applied Geochemistry* **8** (6): 529-549. http://dx.doi.org/10.1016/0883-2927(93)90012-6.

Brons, Glen, Yu, Jimmy M. 1995. Solvent Deasphalting Effects on Whole Cold Lake Bitumen. *Energy & Fuels* **9** (4): 641-647. 10.1021/ef00052a011.

Buckley, Jill S. 1999. Predicting the Onset of Asphaltene Precipitation from Refractive Index Measurements. *Energy & Fuels* **13** (2): 328-332. 10.1021/ef980201c.

Buenrostro-Gonzalez, E., Lira-Galeana, C., Gil-Villegas, A. et al. 2004. Asphaltene Precipitation in Crude Oils: Theory and Experiments. *American Institute of Chemical Engineers* **50** (10): 2552-2570.

Calemma, V., Iwanski, P., Nali, M. et al. 1995. Structural Characterization of Asphaltenes of Different Origins. *Energy & Fuels* **9** (2): 225-230. 10.1021/ef00050a004.

Carbognani, L., Orea, M., Fonseca, M. 1999. Complex Nature of Separated Solid Phases from Crude Oils. *Energy & Fuels* **13** (2): 351-358. 10.1021/ef9801975.

Carnahan, N.F., Salager, J., Anton, R. et al. 1999. Properties of Resins Extracted from Boscan Crude Oial and Their Effect on the Stability of Asphaltenes in Boscan and Hamacan Crude Oils. *Energy Fuels* **13** (2): 309-314.

Castro, L.V., Vazquez, F. 2009. Fractionation and Characterization of Mexican Crude Oils. *Energy Fuels* **23** (3): 1603-1609.

Chan, K. L. Andrew, Kazarian, Sergei G. 2006. Detection of trace materials with Fourier transform infrared spectroscopy using a multi-channel detector. *Analyst* **131** (1): 126-131. 10.1039/B511243E.

Clayden, J. 2001. *Organic Chemistry*. Oxford, New York, Oxford University Press.

Dabir, Bahram, Nematy, Mehdi, Mehrabi, Ali Reza et al. 1996. Asphalt flocculation and deposition. III. The molecular weight distribution. *Fuel* **75** (14): 1633-1645. http://dx.doi.org/10.1016/S0016-2361(96)00153-6.

Dunning, H. N., Rabon, Nancy A. 1956. Porphyrin-Metal Complexes in Petroleum Stocks. *Industrial & Engineering Chemistry* **48** (5): 951-955. 10.1021/ie50557a040.

Erickson, R. L., Myers, A. T., Horr, C. A. 1954. Association of Uranium and Other Metals with Crude Oil, Asphalt, and Petroliferous Rock. *AAPG Bulletin* **38** (10): 2200-2218.

Fan, T., Buckley, J.S. 2002. Rapid and Accurate SARA Analysis of Medium Gravity Crude Oils. *Energy Fuels* **16** (6): 1571-1575.

Fish, Richard H., Komlenic, John J., Wines, Brian K. 1984. Characterization and comparison of vanadyl and nickel compounds in heavy crude petroleums and asphaltenes by reverse-phase and size-exclusion liquid chromatography/graphite furnace atomic absorption spectrometry. *Analytical Chemistry* **56** (13): 2452-2460. 10.1021/ac00277a043.

Fuhr, B.J., Holloway, L.R. 1999. Analytical Considerations Related to Asphaltenes and Waxes in the Same Crudes. *Energy Fuels* **13** (2): 336-339.

Furimsky, Edward. 1978. Chemical Origin of Coke Deposited on Catalyst Surface. *Industrial & Engineering Chemistry Product Research and Development* **17** (4): 329-331. 10.1021/i360068a008.

Gaspar, A., Zellermann, E., Labbidi, S. et al. 2012. Characterization of Saturates, Aromatics, Resins, and Asphaltenes Heavy Crude Oil Fractions by Atmospheric Pressure Laser Ionization Fourier Transform Ion Cyclotron Resonance Mass Spectrometry. *Energy Fuels* **26** (6): 3481-3487.

Gawel, I., Speight, J.G. 2010. Chapter 2. Effect of Asphaltene Constituents on Refinery Processes and Products. In *Asphaltenes: Characterization, Properties and Applications*, ed. J.A. Duncan, 47-79. New York, Nova Science Publishers.

Goual, L., Firoozabadi, A. 2002. Measuring asphaltenes and resins, and dipole moment in petroleum fluids. *AIChE Journal* **48** (11): 2646-2663.

Goual, L., Sedghi, M., Mostowfi, F. et al. 2014. Cluster of Asphaltene Nanoaggregates by DC Conductivity and Centrifugation. *Energy Fuels* **28** (8): 5002-5013.

Green, J. B., Yu, S. K. T., Pearson, C. D. et al. 1993. Analysis of sulfur compound types in asphalt. *Energy & Fuels* **7** (1): 119-126. 10.1021/ef00037a019.

Groen, John C., Craig, James R. 1994. The inorganic geochemistry of coal, petroleum, and their gasification/combustion products. *Fuel Processing Technology* **40** (1): 15-48. http://dx.doi.org/10.1016/0378-3820(94)90033-7.

Hammami, A., Phelps, C.H., Monger-McClure, T. et al. 2000. Asphaltene Precipitation from Live Oils: An Experimental Investigation of Onset Conditions and Reversibility. *Energy Fuels* **14** (1): 14-18.

Hannisdal, A., Ese, M., Hemmingsen, P.V. et al. 2006. Particle-stabilized emulsions: Effect of heavy crude oil components pre-adsorbed onto stabilizing solids.

Colloids and Surfaces A: Physicochemical and Engineering Aspects **276** (1-3): 45-58.

He, L., Li, X., Wu, G. et al. 2013. Distribution of Saturates, Aromatics, Resins, and Asphaltenes Fractions in the Bituminous Layer of Athabasca Oil Sands. *Energy Fuels* **27** (8): 4677-4683.

Hildebrand, Joel H. 1919. SOLUBILITY. III. RELATIVE VALUES OF INTERNAL PRESSURES AND THEIR PRACTICAL APPLICATION. *Journal of the American Chemical Society* **41** (7): 1067-1080. 10.1021/ja02228a004.

Ignasiak, Teresa, Strausz, Otto P., Montgomery, Douglas S. 1977. Oxygen distribution and hydrogen bonding in Athabasca asphaltene. *Fuel* **56** (4): 359-365. http://dx.doi.org/10.1016/0016-2361(77)90059-X.

Manual of Petroleum Measurement Standards. Chapter 11.1 — Temperature and Pressure Volume Correction Factors for Generalized Crude Oils, Refined Products, and Lubricating Oils. 2004. Washington D.C.: American Petroleum Institute.

Izquierdo, A., Rivas, O. 1997. A Global Approach to Asphaltene Deposition Problems. Presented at SPE International Symposium on Oilfield Chemistry, Houston, Texas, 18-21 February. SPE-37251-MS. http://dx.doi.org/10.2118/37251-MS.

Jada, A., Salou, M. 2002. Effects of the asphaltene and resin contents of the bitumens on the water–bitumen interface properties. *Journal of Petroleum Science and Engineering* **33** (1-3): 185-193.

Jamaluddin, A. K. M., Nazarko, T. W., Sills, Suzanne et al. 1996. Deasphalted Oil - A Natural Asphaltene Solvent. *SPE Production & Facilities* **11** (03): 161-165. 10.2118/28994-PA.

Kaminski, Thomas J., Fogler, H. Scott, Wolf, Nick et al. 2000. Classification of Asphaltenes via Fractionation and the Effect of Heteroatom Content on Dissolution Kinetics. *Energy & Fuels* **14** (1): 25-30. 10.1021/ef990111n.

Kar, T., Hascakir, B. 2015. The Role of Resins, Asphaltenes, and Water in Water–Oil Emulsion Breaking with Microwave Heating. *Energy Fuels* **29** (6): 3684-3690.

Kar, T., Williamson, M., Hascakir, B. 2014. The Role of Asphaltenes in Emulsions Formation for Steam Assisted Gravity Drainage (SAGD) and Expanding

Solvent-SAGD (ES-SAGD). Presented at SPE Heavy and Extra Heavy Oil Conference - Latin America, Medellin, Colombia, 24-26 September. SPE-171076-MS. http://dx.doi.org/10.2118/171076-MS.

Khalifeh, M., Kharrat, R., Bagherzadeh, H. et al. 2013. An Experimental and Simulation Study of Asphaltene-Induced Permeability Impairment under Natural Depletion Condition. Presented at SPE European Formation Damage Conference and Exhibition, Noordwijk, The Netherlands, 5-7 June 2013. SPE-165196-MS. http://dx.doi.org/10.2118/165196-MS.

Kharrat, A.M., Zacharia, J., Cherian, V.J. et al. 2007. Issues with Comparing SARA Methodologies. *Energy Fuels* **21** (6): 3618-3621.

Klein, Geoffrey C., Kim, Sunghwan, Rodgers, Ryan P. et al. 2006. Mass Spectral Analysis of Asphaltenes. I. Compositional Differences between Pressure-Drop and Solvent-Drop Asphaltenes Determined by Electrospray Ionization Fourier Transform Ion Cyclotron Resonance Mass Spectrometry. *Energy & Fuels* **20** (5): 1965-1972. 10.1021/ef0600199.

Klein, Joseph C., Hercules, David M. 1983. Surface characterization of model Urushibara catalysts. *Journal of Catalysis* **82** (2): 424-441. http://dx.doi.org/10.1016/0021-9517(83)90209-9.

Kokal, S. L., Najman, J., Sayegh, S. G. et al. 1992. Measurement And Correlation Of Asphaltene Precipitation From Heavy Oils By Gas Injection. 10.2118/92-04-01.

Kokal, S.L., Sayegh, S.G. 1995. Asphaltenes: The Cholesterol of Petroleum. Presented at SPE Middle East Oil Show, Bahrain. SPE-29787-MS. http://dx.doi.org/10.2118/29787-MS.

Krump, H., Alexy, P., Luyt, A.S. 2005. Preparation of a maleated Fischer-Tropsch paraffin wax and FTIR analysis of grafted maleic anhydride. *Polymer Testing* **24** (2): 129-135.

Larkin, Peter. 2011. Chapter 6 - IR and Raman Spectra-Structure Correlations: Characteristic Group Frequencies. In *Infrared and Raman Spectroscopy*, ed. Peter Larkin, 73-115. Oxford, Elsevier.

Lee, Thomas W. 2002. *Microelectronic Failure Analysis: Desk Reference 2002 Supplement*, 4th ed. edition, 5. Materials Park, Ohio, USA, ASM International.

Leontaritis, K.J. 1989. Asphaltene Deposition: A Comprehensive Description of Problem Manifestations and Modeling Approaches. Presented at SPE Production Operations Symposium, Oklahoma City, Oklahoma, March 13-14. SPE-18892-MS. http://dx.doi.org/10.2118/18892-MS.

Leontaritis, K.J., Amaefule, J.O., Charles, R.E. 1994. A Systematic Approach for the Prevention and Treatment of Formation Damage Caused by Asphaltene Deposition. *SPE Production & Facilities* **9** (03): 157-164. SPE-23810-PA. http://dx.doi.org/10.2118/23810-PA.

Li, Kejing, McAlpin, Casey R., Akeredolu, Babajade A. et al. 2012. A Rheological and Chemical Investigation of Canadian Heavy Oils From the McMurray Formation. *Energy & Fuels* **26** (7): 4445-4453. 10.1021/ef300608w.

Li, Zhidong, Firoozabadi, Abbas. 2010. Modeling Asphaltene Precipitation by n-Alkanes from Heavy Oils and Bitumens Using Cubic-Plus-Association Equation of State. *Energy & Fuels* **24** (2): 1106-1113. 10.1021/ef9009857.

Lian, H., Lin, J., Yen, T.F. 1994. Peptization studies of asphaltene and solubilty parameter spectra. *Fuel* **73** (3): 423-428.

Limanowka, W.A., Voytechek, M.J., Limanowka, R.E. 1999. Asphaltene Deposition Problems in Oil Industry with Focus on Electric Submersible Pump Applications. Presented at SPE Annual Technical Conference and Exhibition, Houston, Texas, 3-6 October. SPE-56662-MS. http://dx.doi.org/10.2118/56662-MS.

Loeber, L., Muller, G., Morel, J. et al. 1998. Bitumen in colloid science: a chemical, structural and rheological approach. *Fuel* **77** (13): 1443-1450.

Manahan, Stanley E. 1990. *Hazardous Waste Chemistry, Toxicology, and Treatment*. Michigan, CRC Press.

McCain, W.D., Jr. 1990. *The Properties of Petroleum Fluids*, 2nd ed. edition. Tulsa, Oklahoma, PennWell Publishing Company.

McKenna, Amy M., Purcell, Jeremiah M., Rodgers, Ryan P. et al. 2009. Identification of Vanadyl Porphyrins in a Heavy Crude Oil and Raw Asphaltene by Atmospheric Pressure Photoionization Fourier Transform Ion Cyclotron Resonance (FT-ICR) Mass Spectrometry. *Energy & Fuels* **23** (4): 2122-2128. 10.1021/ef800999e.

McLean, Joseph D., Kilpatrick, Peter K. 1997. Comparison of Precipitation and Extrography in the Fractionation of Crude Oil Residua. *Energy & Fuels* **11** (3): 570-585. 10.1021/ef9601125.

Meyer, R.F., de Witt, W., Jr. 1990. *Definition and world resources of natural bitumens*. Denver, CO: U.S. Geological Survey Bulletin 1944, Department of the Interior, U.S. Geological Survey.

Mitchell, D.L., Speight, J.G. 1973. The solubility of asphaltenes in hydrocarbon solvents. *Fuel* **52** (2): 149-152.

Moschopedis, Speros E., Speight, James G. 1975. Oxidation of a bitumen. *Fuel* **54** (3): 210-212. http://dx.doi.org/10.1016/0016-2361(75)90014-9.

Moschopedis, Speros E., Speight, James G. 1976a. Investigation of hydrogen bonding by oxygen functions in Athabasca bitumen. *Fuel* **55** (3): 187-192. http://dx.doi.org/10.1016/0016-2361(76)90086-7.

Moschopedis, Speros E., Speight, James G. 1976b. Oxygen functions in asphaltenes. *Fuel* **55** (4): 334-336. http://dx.doi.org/10.1016/0016-2361(76)90035-1.

Mukhametshina, A., Kar, T., Hascakir, B. 2015. Asphaltene Precipitation during Bitumen Extraction with Expanding Solvent Steam Assisted Gravity Drainage (ES-SAGD): Effects on Pore-Scale Displacement. *SPE Journal*. SPE-170013-PA. http://dx.doi.org/10.2118/170013-PA.

Mullins, O.C., Seifert, D.J., Zue, J.Y. et al. 2013. Clusters of Asphaltene Nanoaggregates Observed in Oilfield Reservoirs. *Energy Fuels* **27** (4): 1752-1761.

Mullins, O.C., Sheu, E.Y., Hammami, A. et al. 2007. *Asphaltenes, Heavy Oils, and Petroleomics*. New York, Springer Science and Publishing Media.

Musser, B.J., Kilpatrick, P.K. 1998. Molecular Characterization of Wax Isolated from a Variety of Crude Oils. *Energy & Fuels* **12** (4): 715-725.

Nalwaya, Vaibhav, Tantayakom, Veerapat, Piumsomboon, Pornpote et al. 1999. Studies on Asphaltenes through Analysis of Polar Fractions. *Industrial & Engineering Chemistry Research* **38** (3): 964-972. 10.1021/ie9804428.

Ortega, L.C., Rogel, E., Vien, J. et al. 2015. Effect of Precipitating Conditions on Asphaltene Properties and Aggregation *Energy Fuels* **29** (6): 3664-3674.

Parra-Barraza, H., Hernandez-Montiel, D., Lizardi, J. et al. 2003. The zeta potential and surface properties of asphaltenes obtained with different crude oil/n-heptane proportions. *Fuel* **82**: 869-874.

Pereira, J.C., Delgado-Linares, J., Briones, A. et al. 2011. The Effect of Solvent Nature and Dispersant Performance on Asphaltene Precipitation from Diluted Solutions of Instable Crude Oil. *Petroleum Science and Technology* **29**: 2432-2440.

Prakoso, A.A., Punase, A.D., Hascakir, B. 2015. A Mechanistic Understanding of Asphaltene Precipitation from Varying Saturate Concentration Perspective. Presented at SPE Latin American and Carribean Petroleum Engineering Conference, Quito, Ecuador, 18-20 November. SPE-177280-MS.

Prakoso, Andreas, Klock, Kristina, Punase, Abhishek et al. 2016. Determination of the Stability of Asphaltenes through Physicochemical Characterization of Asphaltenes. Presented at SPE Western Regional Meeting, Anchorage, Alaska, USA, 23-26 May. SPE 180422-MS.

Punase, Abhishek, Prakoso, Andreas, Hascakir, Berna. 2016. The Polarity of Crude Oil Fractions Affects the Asphaltenes Stability. Presented at SPE Western Regional Meeting, Anchorage, Alaska, USA, 23-26 May. SPE-180423-MS.

Quaroni, Luca, Chumanov, George. 1999. Preparation of Polymer-Coated Functionalized Silver Nanoparticles. *Journal of the American Chemical Society* **121** (45): 10642-10643. 10.1021/ja992088q.

Ramos, A.C.S., Haraguchi, L., Notrispe, F.R. et al. 2001. Interfacial and colloidal behavior of asphaltenes obtained from Brazilian crude oils. *Journal of Petroleum Science and Engineering* **32**: 201-216.

Rappoport, Z. 2003. *The chemistry of phenols*. Chichester, England ; Hoboken, NJ, Wiley.

Ravey, J.C., Ducouret, G., Espinat, D. 1988. Asphaltene macrostructure by small angle neutron scattering. *Fuel* **67** (11): 1560-1567.

Redelius, P., Soenen, H. 2015. Relation between bitumen chemistry and performance. *Fuel* **140**: 34-43.

Reichardt, C. 1988. *Solvents and solvent effects in organic chemistry*. Weinheim, Federal Republic of Germany ; New York, NY, USA, VCH.

Riddick, T. 1968. *Control of Colloid Stability through Zeta Potential With a closing chapter on its relationship to cardiovascular disease*. Wynnewood, PA, Zeta-Meter Inc.

Rogel, E., Carbognani, L. 2003. Density Estimation of Asphaltenes Using Molecular Dynamics Simulations. *Energy Fuels* **17** (2): 378-386.

Rogel, E., Ovalles, C., Moir, M. 2010. Asphaltene Stability in Crude Oils and Petroleum Materials by Solubility Profile Analysis. *Energy Fuels* **24**: 4369-4374.

Rogel, E., Ovalles, C., Moir, M. 2012. Asphaltene Chemical Characterization as a Function of Solubility: Effects on Stability and Aggregation. *Energy Fuels* **26** (5): 2655-2662.

Rogel, E., Roye, M., Vien, J. et al. 2015. Characterization of Asphaltene Fractions: Distribution, Chemical Characteristics, and Solubility Behavior. *Energy Fuels* **29** (4): 2143-2152.

Rogel, Estrella, Miao, Toni, Vien, Janie et al. 2015. Comparing asphaltenes: Deposit versus crude oil. *Fuel* **147**: 155-160. http://dx.doi.org/10.1016/j.fuel.2015.01.045.

Ruiz-Morales, Yosadara. 2002. HOMO−LUMO Gap as an Index of Molecular Size and Structure for Polycyclic Aromatic Hydrocarbons (PAHs) and Asphaltenes: A Theoretical Study. I. *The Journal of Physical Chemistry A* **106** (46): 11283-11308. 10.1021/jp021152e.

Ruiz-Morales, Yosadara, Mullins, Oliver C. 2007. Polycyclic Aromatic Hydrocarbons of Asphaltenes Analyzed by Molecular Orbital Calculations with Optical Spectroscopy. *Energy & Fuels* **21** (1): 256-265. 10.1021/ef060250m.

Salgın, Sema, Salgın, Uğur, Bahadır, Seda. 2012. Zeta Potentials and Isoelectric Points of Biomolecules: The Effects of Ion Types and Ionic Strengths. *Int. J. Electrochem. Sci.* **7**: 12404-12414.

Sastry, M. I. S., Chopra, Anju, Sarpal, A. S. et al. 1998. Determination of Physicochemical Properties and Carbon-Type Analysis of Base Oils Using Mid-IR Spectroscopy and Partial Least-Squares Regression Analysis. *Energy & Fuels* **12** (2): 304-311. 10.1021/ef970125y.

Schlotter, N. E., Porter, Marc D., Bright, T. B. et al. 1986. Formation and structure of a spontaneously adsorbed monolayer of arachidic on silver. *Chemical Physics Letters* **132** (1): 93-98. http://dx.doi.org/10.1016/0009-2614(86)80702-3.

Seifried, C.M., Lawati, S.A., Crawshaw, J.P. et al. 2013. Asphaltene Deposition in Capillary Flow. Presented at SPE Annualt Technical Conference and Exhibition, New Orleans, Lousiana, USA, 30 September - 2 October 2013. SPE-166289-MS. http://dx.doi.org/10.2118/166289-MS.

Siddiqui, M. N., Ali, M. F. 1999. Studies on the aging behavior of the Arabian asphalts. *Fuel* **78** (9): 1005-1015. http://dx.doi.org/10.1016/S0016-2361(99)00018-6.

Silverstein, Robert M., Bassler, G. Clayton. 1967. *Spectrometric identification of organic compounds*, 2nd edition. New York, John Wiley & Sons, Inc.

Sirota, E.B. 2005. Physical Structure of Asphaltenes. *Energy Fuels* **19** (4): 1290-1296.

Skoog, D.A., West, D.M., Holler, F.J. et al. 2014. *Fundamentals of analytical chemistry*, 9 edition. Belmont, CA, Brooks/Cole, Cengage Learning.

Snyder, L. R., Buell, B. E., Howard, H. E. 1968. Nitrogen and oxygen compound types in petroleum. Total analysis of a 700-850.deg.F. distillate from a California crude oil. *Analytical Chemistry* **40** (8): 1303-1317. 10.1021/ac60264a005.

Speight, J. G. 1994. Chemical and Physical Studies of Petroleum Asphaltenes. In *Developments in Petroleum Science*, ed. T. F. Yen and G. V. Chilingarian, Chap. 2, 7-65. Elsevier.

Speight, J.G. 2006. *The Chemistry and Technology of Petroleum*. New York, USA, CRC Press (Reprint).

Speight, J.G., Long, R.B. 1996. The Concept of Asphaltenes Revisited. *Fuel Science and Technology International* **14** (1-2): 1-12.

Speight, J.G., Long, R.B., Trowbridge, T.D. 1984. Factors influencing the separation of asphaltenes from heavy petroleum feedstocks. *Fuel* **63**: 616-620.

Speight, James G. 2014. *Chemical Industries : Chemistry and Technology of Petroleum (5th Edition)*. Boca Raton, FL, USA, CRC Press.

Speight, James G., Moschopedis, Speros E. 1982. On the Molecular Nature of Petroleum Asphaltenes. In *Chemistry of Asphaltenes*, Chap. 1, 1-15. Advances in Chemistry, American Chemical Society.

Spiecker, P.M., Gawrys, K.L., Trail, C.B. et al. 2003. Effects of petroleum resins on asphaltene aggregation and water-in-oil emulsion formation. *Colloids and Surfaces A: Physicochemical and Engineering Aspects* **220** (1-3): 9-27.

Takahashi, Akihisa, Torigoe, Takahiro. 2008. Oil Sands Reservoir Characterization in Athabasca, Canada. Presented at International Petroleum Technology Conference, Kuala Lumpur, Malaysia, 3-5 December. IPTC-12205-MS. 10.2523/12205-MS.

Tang, Guo-Qing, Morrow, Norman R. 1999. Influence of brine composition and fines migration on crude oil/brine/rock interactions and oil recovery. *Journal of Petroleum Science and Engineering* **24** (2–4): 99-111. http://dx.doi.org/10.1016/S0920-4105(99)00034-0.

Taylor, S.E. 1998. The electrodeposition of asphaltenes and implications for asphaltene structure and stability in crude and residual oils. *Fuel* **77** (8): 821-828.

Tennyson, Jonathan, Bernath, Peter F., Brown, Linda R. et al. 2009. IUPAC critical evaluation of the rotational–vibrational spectra of water vapor. Part I—Energy levels and transition wavenumbers for H217O and H218O. *Journal of Quantitative Spectroscopy and Radiative Transfer* **110** (9–10): 573-596. http://dx.doi.org/10.1016/j.jqsrt.2009.02.014.

Thawer, R., Nicoll, D.C.A., Dick, G. 1990. Asphaltene Deposition in Production Facilities. *SPE Production Engineering* **5** (04): 475-480. SPE-18473-PA. http://dx.doi.org/10.2118/18473-PA.

Uetani, T. 2014. Wettability Alteration by Asphaltene Deposition: A Field Example. Presented at Abu Dhabi International Petroleum Exhibition and Conference, Abu Dhabi, UAE, 10-13 November. SPE-171788-MS. http://dx.doi.org/10.2118/171788-MS.

Unur, Ece. 2013. Functional nanoporous carbons from hydrothermally treated biomass for environmental purification. *Microporous and Mesoporous Materials* **168**: 92-101. http://dx.doi.org/10.1016/j.micromeso.2012.09.027.

Waldo, Geoffrey S., Carlson, Robert M. K., Moldowan, J. Michael et al. 1991. Sulfur speciation in heavy petroleums: Information from X-ray absorption near-edge structure. *Geochimica et Cosmochimica Acta* **55** (3): 801-814. http://dx.doi.org/10.1016/0016-7037(91)90343-4.

Wang, J., Buckley, J.S. 2003. Asphaltene Stability in Crude Oil and Aromatic Solvents - The Influence of Oil Composition. *Energy Fuels* **17** (6): 1445-1451.

Wang, Wei, Efrima, Shlomo, Regev, Oren. 1998. Directing Oleate Stabilized Nanosized Silver Colloids into Organic Phases. *Langmuir* **14** (3): 602-610. 10.1021/la9710177.

Wattana, P., Fogler, H.S., Yen, A. et al. 2005. Characterization of Polarity-Based Asphaltene Subfractions. *Energy Fuels* **19** (1): 101-110.

Weaver, Charles E. 1967. Potassium, illite and the ocean. *Geochimica et Cosmochimica Acta* **31** (11): 2181-2196. http://dx.doi.org/10.1016/0016-7037(67)90060-9.

Wiącek, Agnieszka, Chibowski, Emil. 1999. Zeta potential, effective diameter and multimodal size distribution in oil/water emulsion. *Colloids and Surfaces A: Physicochemical and Engineering Aspects* **159** (2–3): 253-261. http://dx.doi.org/10.1016/S0927-7757(99)00281-2.

Wiehe, I.A. 2012. Asphaltene Solubility and Fluid Compatibility. *Energy Fuels* **26** (7): 4004-4016.

Wiehe, I.A., Yarranton, H.W., Akbarzadeh, K. et al. 2005. The Paradox of Asphaltene Precipitation with Normal Paraffins. *Energy Fuels* **19** (4): 1261-1267.

Wilt, Brian K., Welch, William T., Rankin, J. Graham. 1998. Determination of Asphaltenes in Petroleum Crude Oils by Fourier Transform Infrared Spectroscopy. *Energy & Fuels* **12** (5): 1008-1012. 10.1021/ef980078p.

Wylde, J.J., Slayer, J.J.L. 2010. Development, Testing, and Field Application of a Heavy-Oil Pipeline-Cleaning Chemical: A Cradle-to-Grave Case History. *SPE Projects, Facilities, & Construction* **5** (01): 22-30. SPE-119688-PA. http://dx.doi.org/10.2118/119688-PA.

Yang, Ming. 2011. Measurement of Oil in Produced Water. In *Produced Water*, ed. Kenneth Lee and Jerry Neff, Chap. 2, 57-88. New York, Springer.

Yarranton, H.W., Alboudwarej, H., Jakher, R. 2000. Investigation of Asphaltene Association with Vapor Pressure Osmometry and Interfacial Tension Measurements. *Ind. Eng. Chem. Res.* **39** (8): 2916-2924.

APPENDIX

$$\Delta \boldsymbol{PS} = \boldsymbol{t}(\mathbf{75}\%) - \boldsymbol{t}(\mathbf{25}\%) \quad \textbf{Equation 1}$$

Where:

t(75%) is the time required to elute 75% of the material

t(25%) is the time required to elute 25% of the material

$$\frac{\mathbf{1}}{\boldsymbol{\rho_{mix}}} = \frac{\boldsymbol{w_{solvent}}}{\boldsymbol{\rho_{solvent}}} + \frac{\boldsymbol{w_{asphaltene}}}{\boldsymbol{\rho_{asphaltene}}} \quad \textbf{Equation 2}$$

Where:

ρ is density in g/cc

w is mass fraction

Table A- 1: ASTM method comparison for asphaltene separation

Name	Solvent Type	Crude Amount (g)	Solvent Amount (mL)
ASTM D2007-11	nC_5^*	10	100
ASTM D3279-12	nC_7^*	1	100
HPLC Method	nC_7^{**}	0.8	25

* uses filtration (0.45 microns filter paper)

** uses HPLC

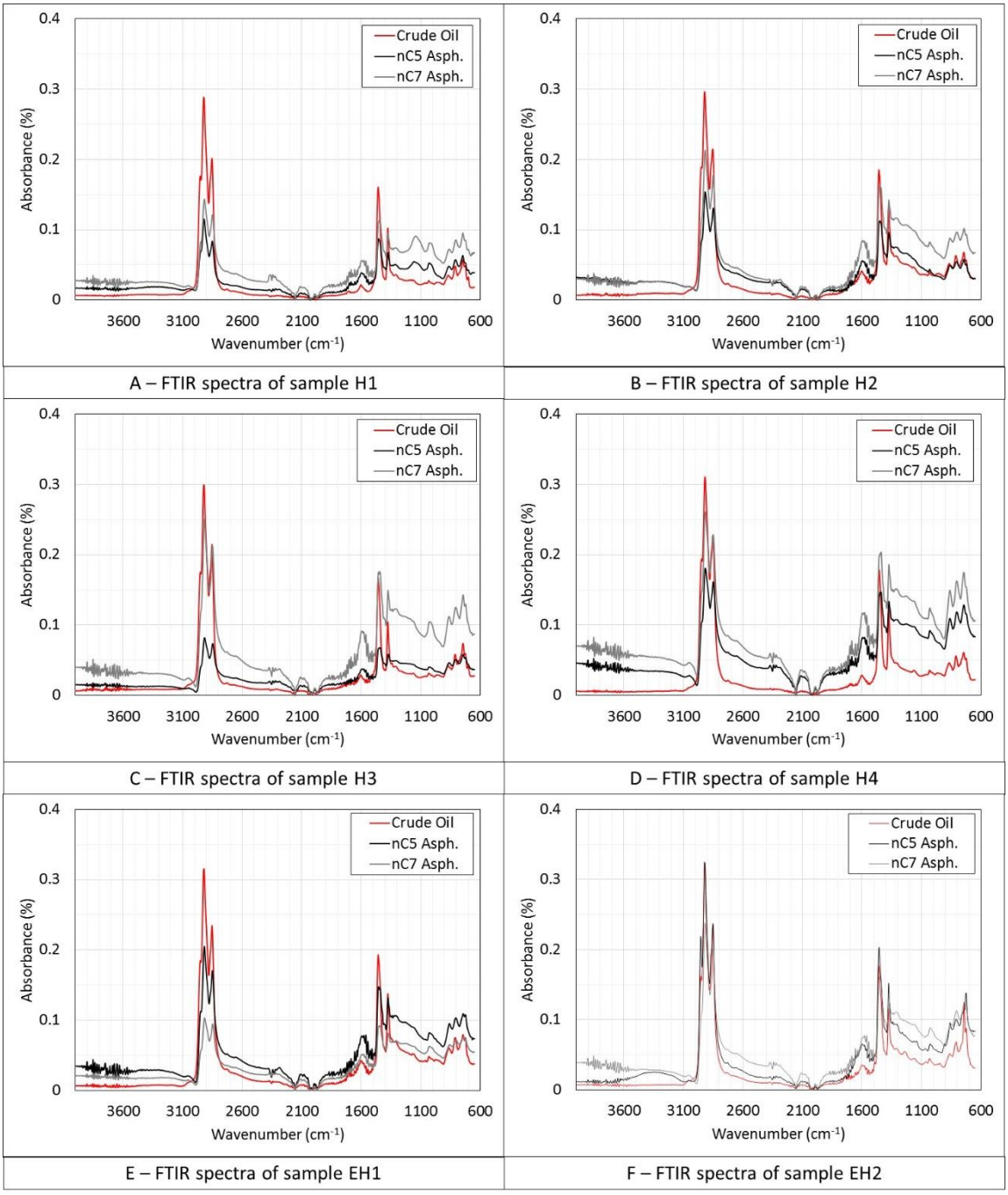

Figure A- 1: FTIR spectra of crude oil and its separated asphaltenes

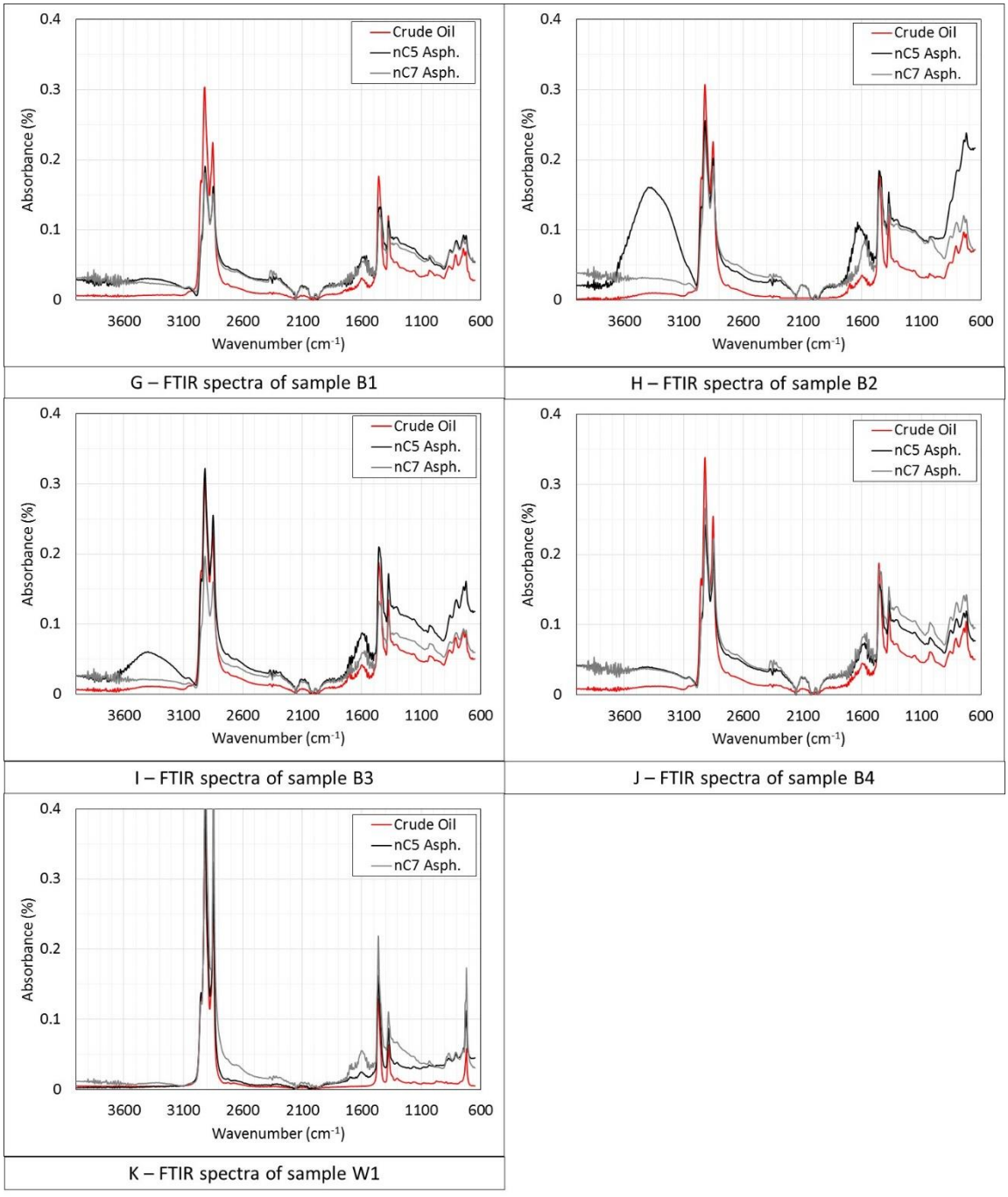

G – FTIR spectra of sample B1

H – FTIR spectra of sample B2

I – FTIR spectra of sample B3

J – FTIR spectra of sample B4

K – FTIR spectra of sample W1

Figure A- 1: Continued

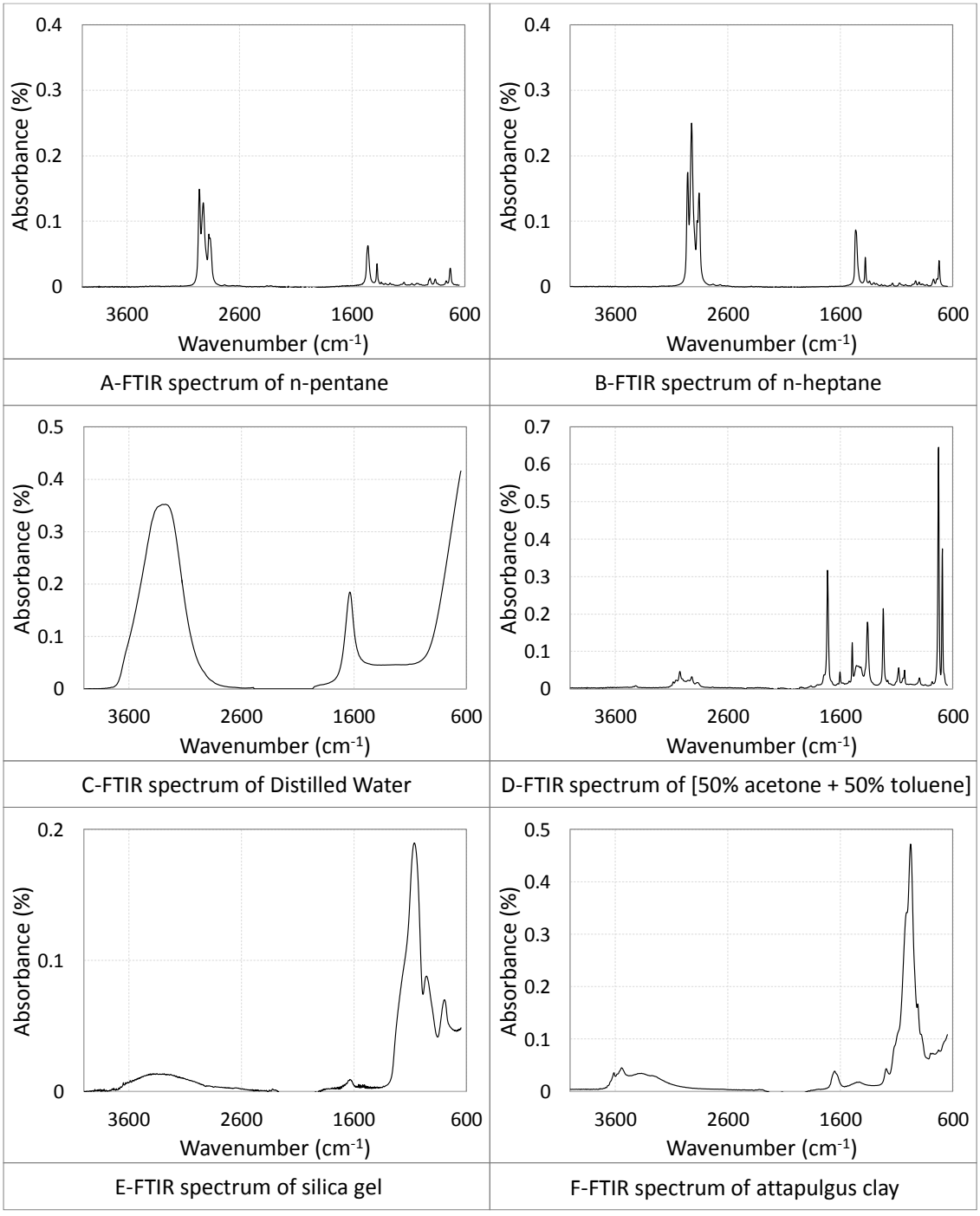

Figure A- 2: FTIR spectra for reference samples

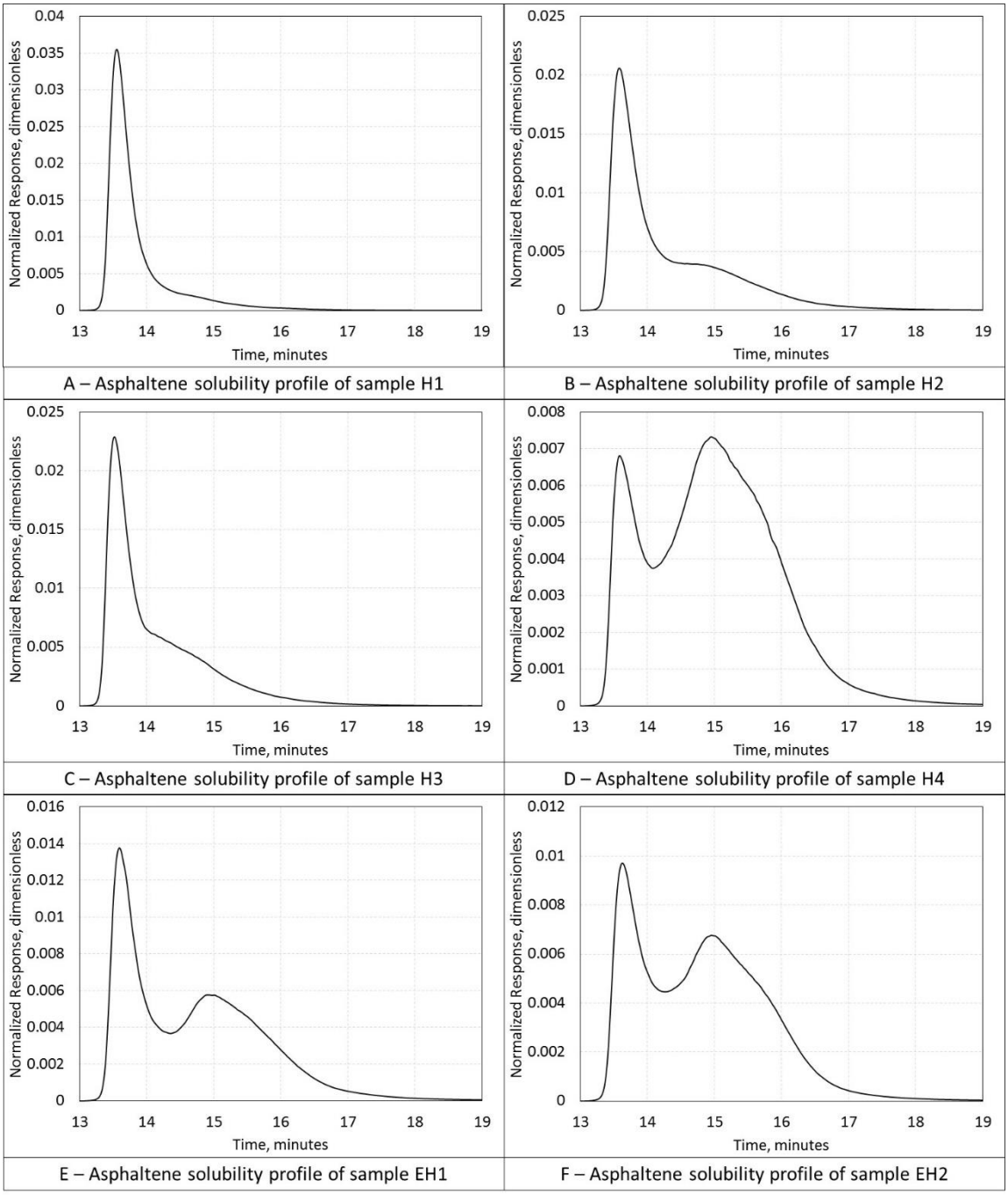

Figure A- 3: Asphaltene solubility profile for crude oil samples

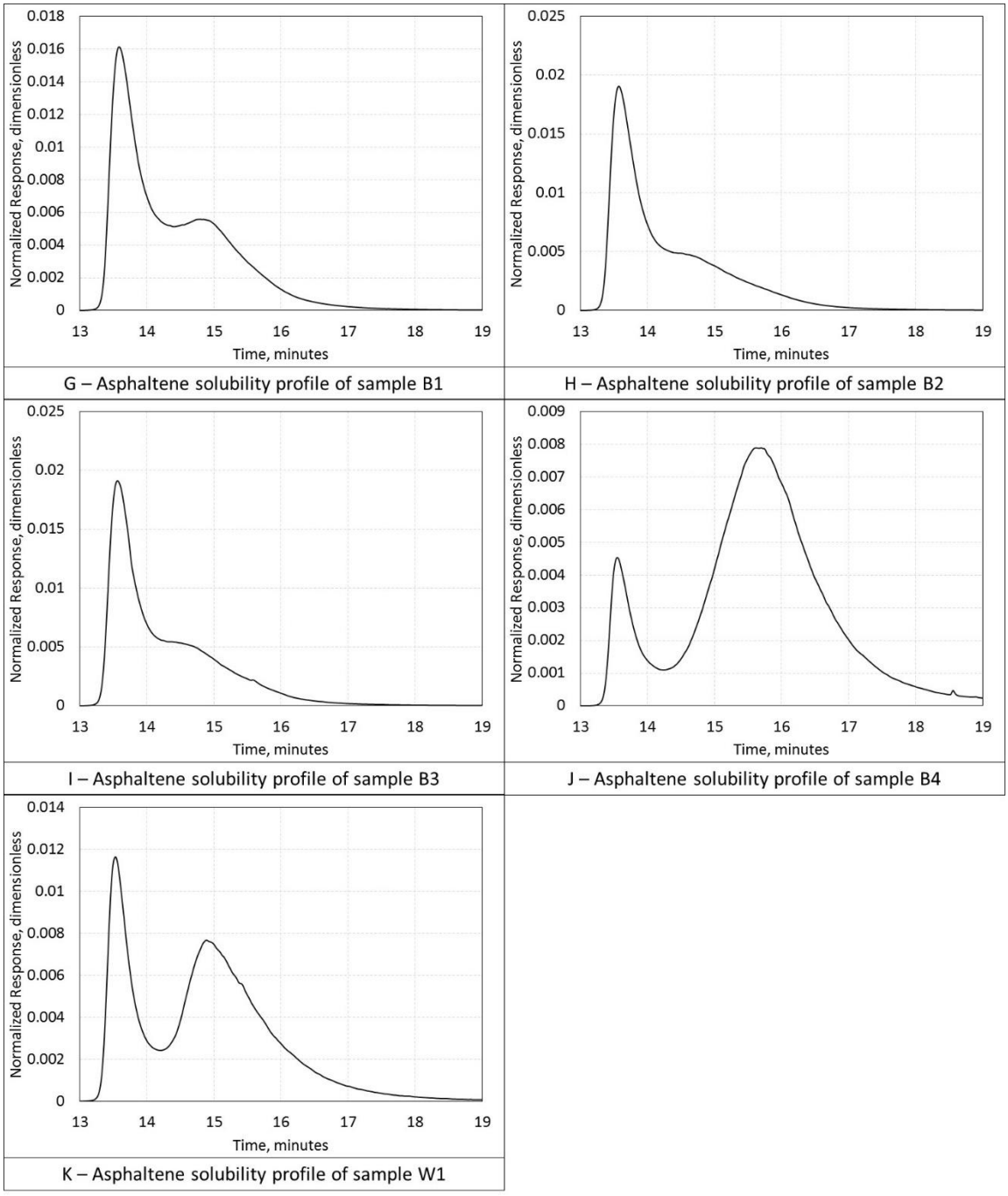

Figure A- 3: Continued

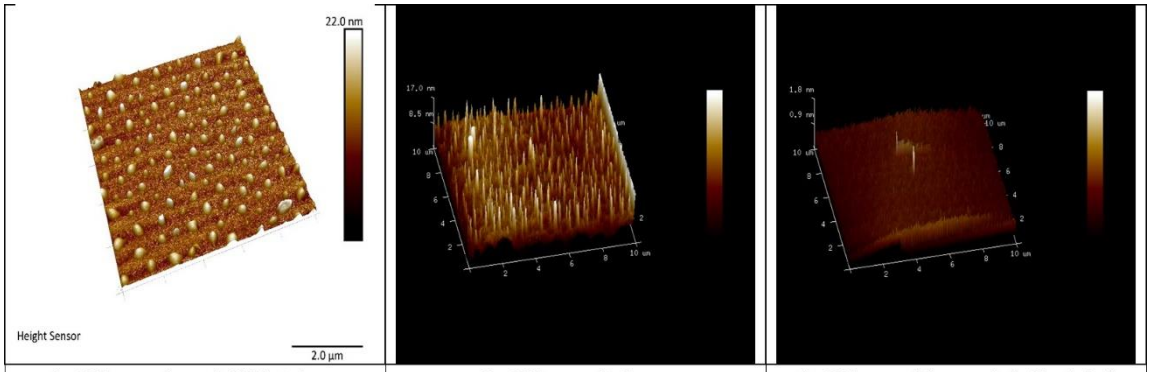

A – 3D image of sample W1 in toluene | B – 3D image of toluene | C – 3D image of the sample holder (mica)

Figure A- 4: Comparison of AFM image of W1 asphaltenes in toluene with reference samples

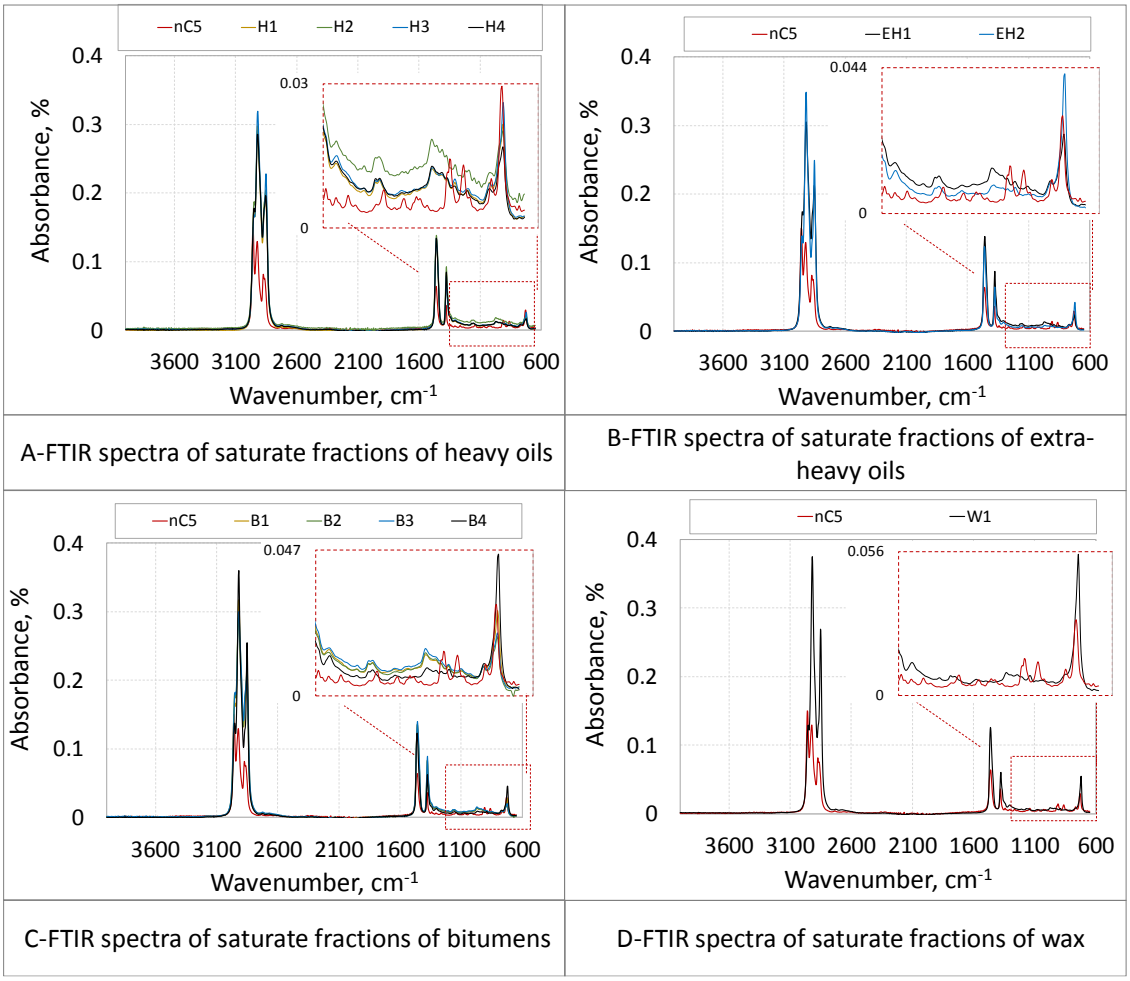

A-FTIR spectra of saturate fractions of heavy oils | B-FTIR spectra of saturate fractions of extra-heavy oils

C-FTIR spectra of saturate fractions of bitumens | D-FTIR spectra of saturate fractions of wax

Figure A- 5: FTIR spectra of the saturate fractions of the bulk samples. The FTIR spectrum for nC5 is provided for comparison purpose since nC5 is a saturated hydrocarbon.

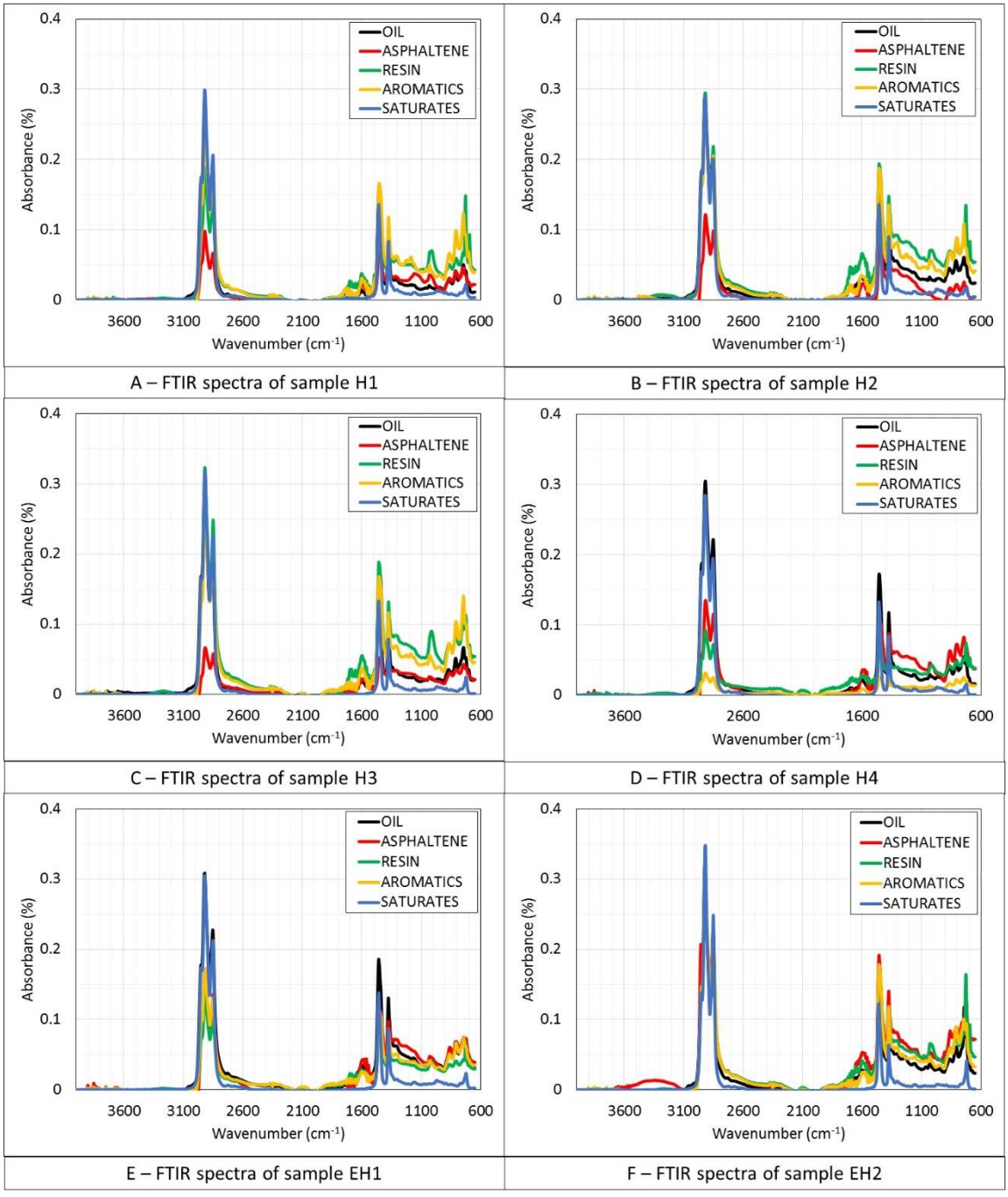

Figure A- 6: FTIR spectra of SARA fractions of 11 different crude oils

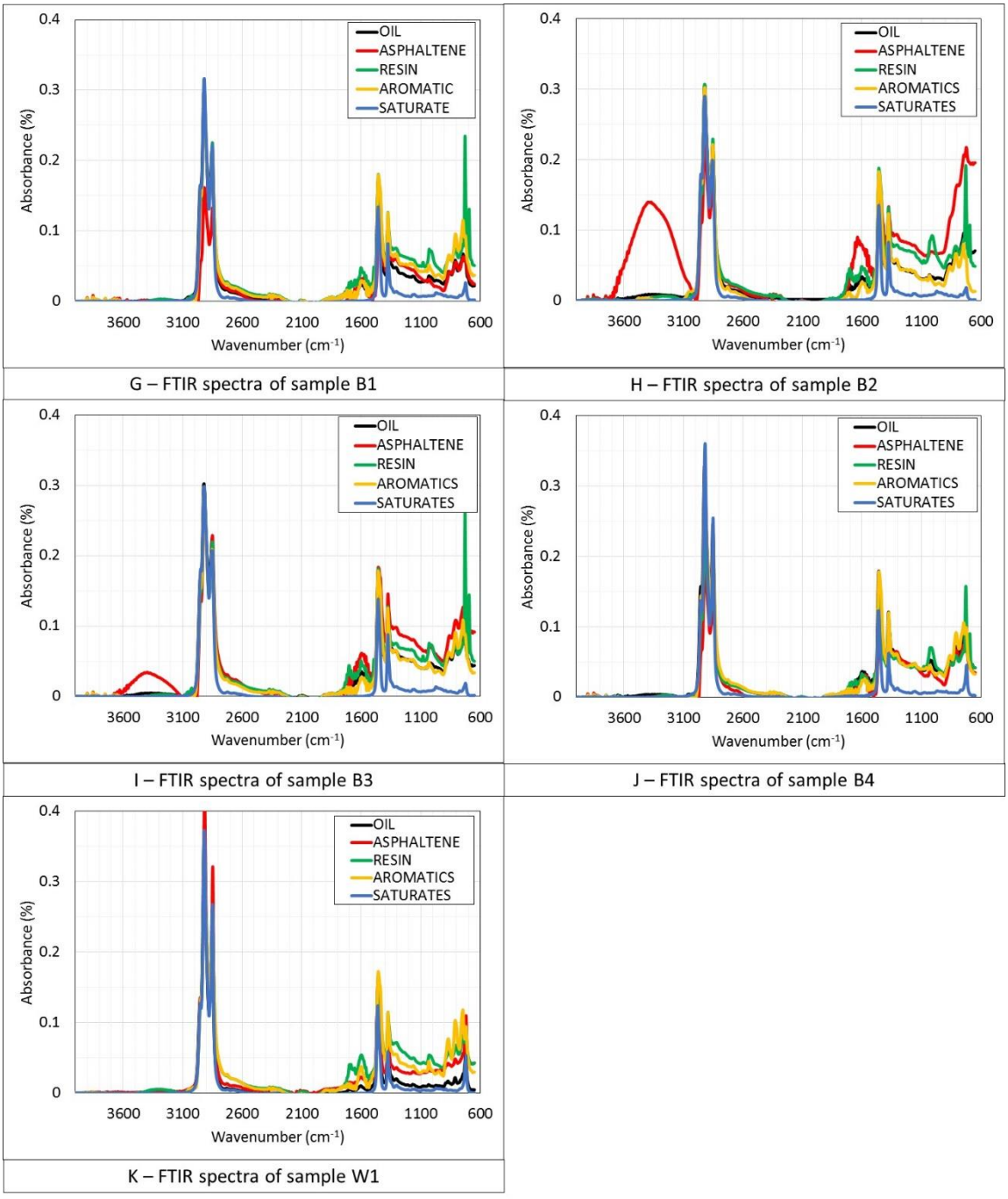

Figure A- 6: Continued

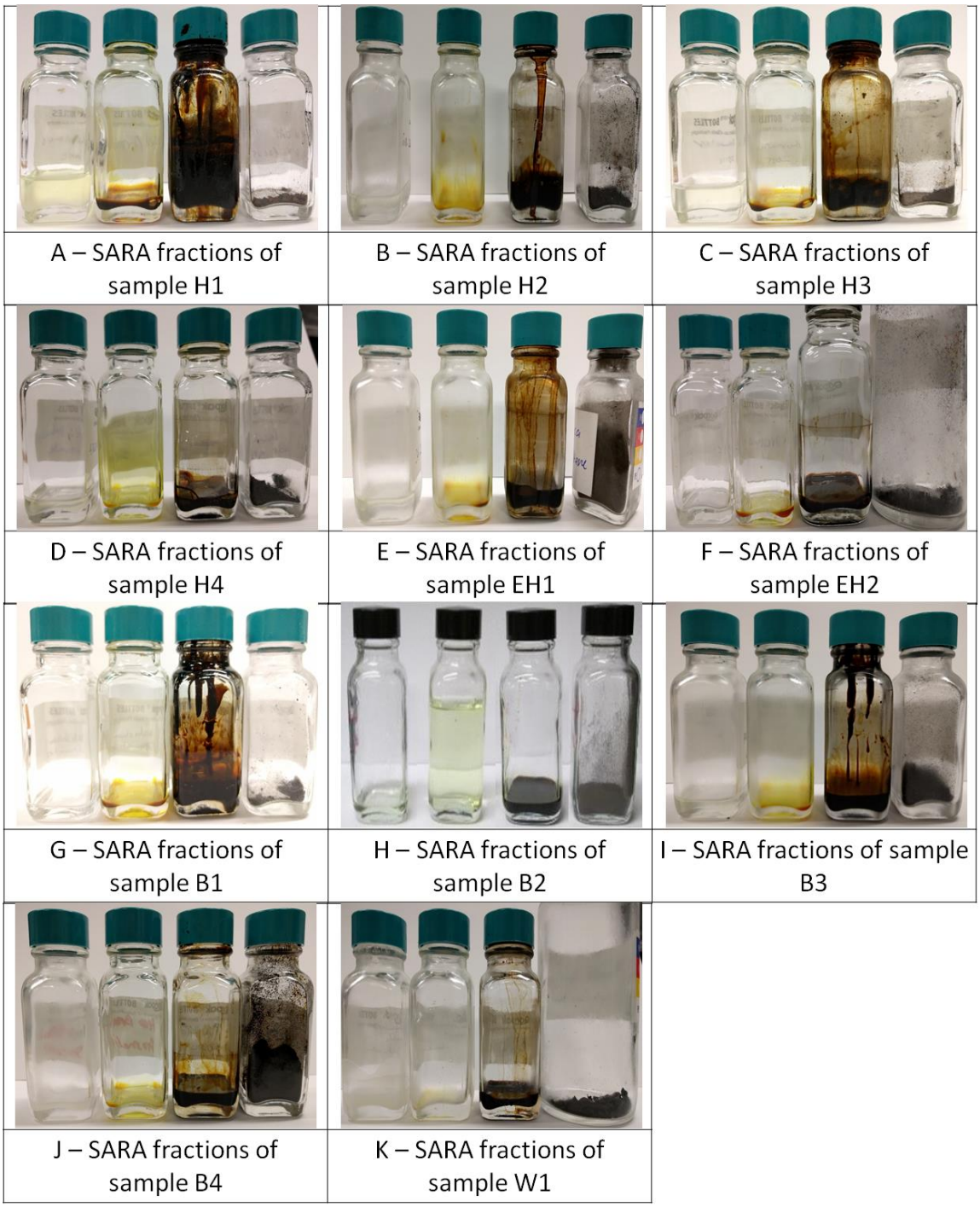

Figure A- 7: SARA fractions of 11 different crude oils